Thesis for the Degree of Doctor of Philosophy

Optical Guiding and Feedback Structures in GaN-Based Vertical-Cavity Surface-Emitting Lasers

Seyed Ehsan Hashemi

Photonics Laboratory
Department of Microtechnology and Nanoscience (MC2)
Chalmers University of Technology
Göteborg, Sweden, 2016

Optical Guiding and Feedback Structures in GaN-Based Vertical-Cavity Surface-Emitting Lasers

Seyed Ehsan Hashemi

Göteborg, December 2016

ISBN 978-91-7597-506-1

Doktorsavhandlingar vid Chalmers Tekniska Högskola
Ny serie 4187
ISSN 0346-718X

Technical Report MC2-350
ISSN 1652-0769

Photonics Laboratory
Department of Microtechnology and Nanoscience - MC2
Chalmers University of Technology
SE-412 96 Göteborg, Sweden
Phone: +46 (0) 31 772 1000

Front cover illustration: (Center) 3D schematic of a GaN VCSEL structure with hybrid epitaxial/dielectric DBRs. (Left) The antiguiding effect of a depressed structure shown by an SEM image and a leaky intracavity field. (Right) Feedback structures of an HCG and a conductive DBR with interlayers.

Printed by Chalmers reproservice, Chalmers University of Technology
Göteborg, Sweden, December, 2016

Optical Guiding and Feedback Structures in GaN-Based Vertical-Cavity Surface-Emitting Lasers

Seyed Ehsan Hashemi
Photonics Laboratory
Department of Microtechnology and Nanoscience - MC2
Chalmers University of Technology
SE-412 96 Göteborg, Sweden

Abstract

The Vertical-Cavity Surface-Emitting Laser (VCSEL) made from GaAs-based materials is an established infrared light source, and is produced in large volumes for short-distance optical links, computer mice, and thermal processing systems. A wide range of applications, such as high-resolution printing, general lighting, and biomedical diagnosis and treatment could benefit from using a VCSEL with blue or ultraviolet emission. A promising solution is the use of GaN-based materials, where only a few research groups have so far demonstrated electrically pumped GaN VCSELs with optical output powers in the milliwatt-range and threshold current densities <10 kA/cm^2, unfortunately though the devices degrade after a few minutes. The major challenges are achieving broadband high-reflectivity mirrors, vertical and lateral carrier confinement, efficient lateral current spreading, accurate cavity length control, and lateral optical mode confinement.

This thesis is focused on exploring the lateral optical guiding and feedback structures for GaN VCSELs. By numerical simulations, the most commonly used GaN VCSEL cavities were investigated and it was shown that many structures used for lateral current confinement result in unintentionally anti-guided resonators with associated high optical losses. Such resonators have a built-in modal discrimination but the threshold gain is highly dependent on nanometer-sized changes in the structure. In addition, the anti-guided resonators have a strong temperature dependent characteristic, since thermal lensing suppresses the lateral optical leakage. Both distributed Bragg reflectors (DBRs) and high contrast gratings (HCGs) were explored as optical feedback structures. The effect of compositional interlayers on the vertical electrical conductivity of Si-doped AlN/GaN DBRs was investigated. The DBR with no interlayers showed state-of-the-art resistivity for an AlN/GaN DBR as low as 0.044 Ωcm^2 for 8 mirror pairs. The DBRs with compositional interlayers had resistivities between 0.16–0.34 Ωcm^2, indicating that the incorporation of interlayers can impair the vertical current transport. An alternative to a DBR, a high contrast grating (HCG) in TiO_2/air was demonstrated for the first time. The fabricated HCG showed a high reflectivity of >95 % over a 25 nm wavelength span.

Keywords: vertical-cavity surface-emitting laser, gallium nitride, current aperture, optical antiguiding, TiO_2, high contrast grating, conductive DBR, thermal lensing

List of Papers

This thesis is based on the following appended papers:

[A] **E. Hashemi**, J. Gustavsson, J. Bengtsson, M. Stattin, G. Cosendey, N. Grandjean, and Å. Haglund, "Engineering the Lateral Optical Guiding in Gallium Nitride-Based Vertical-Cavity Surface-Emitting Laser Cavities to Reach the Lowest Threshold Gain," *Japanese Journal of Applied Physics*, vol. 52, no. 8S, p. 08JG04, May 2013. doi:10.7567/JJAP.52.08JG04

[B] **E. Hashemi**, J. Bengtsson, J. Gustavsson, M. Stattin, G. Cosendey, N. Grandjean, and Å. Haglund, "Analysis of structurally sensitive loss in GaN-based VCSEL cavities and its effect on modal discrimination," *Optics Express*, vol. 22, no. 1, pp. 411–426, Jan. 2014. doi:10.1364/OE.22.000411

[C] **E. Hashemi**, J. Bengtsson, J. Gustavsson, M. Calciati, M. Goano, and Å. Haglund, "Thermal lensing effects on lateral leakage in GaN-based vertical-cavity surface-emitting laser cavities," Submitted to *Optics Express*, Nov. 2016.

[D] **E. Hashemi**, F. Hjort, M. Stattin, T. Ive, O. Bäcke, M. Halvarsson, V. Desmaris, D. Meledin, and Å. Haglund, "Effect of compositional interlayers on the vertical electrical conductivity of Si-doped AlN/GaN distributed-Bragg reflectors grown on SiC," Submitted to *Applied Physics Letters Photonics*, Nov. 2016.

[E] **E. Hashemi**, J. Bengtsson, J. Gustavsson, S. Carlsson, G. Rossbach and Å. Haglund, "TiO_2 membrane high-contrast grating reflectors for GaN-based vertical-cavity light emitters," *Journal of Vacuum Science & Technology B*, vol. 33, no. 5, p. 050603, Sept. 2015. doi:10.1116/1.4929416

Related conference contributions by the author:

[F] **E. Hashemi**, J. Bengtsson, J. Gustavsson, M. Stattin, M. Glauser, G. Cosendey, N. Grandjean, M. Calciati, M. Goano, and Å. Haglund, "Triggering of guiding and antiguiding effects in GaN-based VCSELs," *Proc. of SPIE, Vertical-Cavity Surface-Emitting Lasers XVIII*, vol. 9001, p. 90010A, Feb. 2014. doi:10.1117/12.2038152

[G] **E. Hashemi**, J. Bengtsson, J. Gustavsson, S. Carlsson, G. Rossbach and Å. Haglund, "Air-suspended TiO_2-based HCG reflectors for visible spectral range," *Proc. of SPIE, High Contrast Metastructures IV*, vol. 9372, p. 93720D, Feb. 2015. doi:10.1117/12.2078951

[H] Å. Haglund, **E. Hashemi**, J. Bengtsson, J. Gustavsson, M. Stattin, M. Calciati, and M. Goano, "Progress and challenges in electrically pumped GaN-based VCSELs," *Proc. of SPIE, Semiconductor Lasers and Laser Dynamics VII*, vol. 9892, p. 98920Y, Apr. 2016. doi:10.1117/12.2229428

[I] F. Hjort, **E. Hashemi**, D. Adolph, T. Ive, and Å. Haglund, "Electrically conductive ZnO/GaN distributed Bragg reflectors grown by hybrid plasma-assisted molecular beam epitaxy," To appear in *Proc. of SPIE, Gallium Nitride Materials and Devices XII*, Feb. 2017.

Acknowledgement

There are many who have supported me and have made my PhD experience a special one. I have had the privilege to work closely with a group of extremely talented people. First of all, I am very grateful to Assoc. Prof. Åsa Haglund for accepting me as her first PhD student to work on an exciting research project. I am thankful to you Åsa for your excellent support and guidance that helped me develop my technical and general skills. You have been a great supervisor and a wonderful role model for me and I have learnt a lot from you to set high goals, be passionate, and work hard to achieve them. I am also very thankful to my co-supervisor Assoc. Prof. Jörgen Bengtsson for his brilliant complementary supervision. Thank you Jörgen for your constant generosity in helping me with the numerical simulations and bringing your deep understanding of optics into the discussions. Thanks also for the pleasant lunch times and your cool and open minded personality. I would like also to thank my other co-supervisor Assoc. Prof. Johan Gustavsson for instructing me with the simulations and always coming up with excellent ideas. Your support has always been valuable for me. My deep gratitude goes to Prof. Anders Larsson, my examiner and head of the Photonics Lab, for his kind support through the last 5 years. I have always been fascinated by his character, vision, and the managerial skills.

I have felt really honored to be a member of the Photonics Lab and have so many wonderful people around in such a lively and pleasant environment. I am thankful to all the past and present members of both the optoelectronics and fiber optics groups. Thanks for all the unforgettable memories. A great deal of appreciation goes to Dr. Martin Stattin, Dr. Rashid Safaisini, and Dr. Erik Haglund, for their time in coaching me to learn the art of cleanroom processing. I am also grateful to the very committed staff of MC2 Nanofabrication Laboratory for their continuous technical support, especially Henrik Frederiksen, Mats Hagberg, Bengt Nilsson, and Piotr Jedrasik. I also thank my two officemates. Michael Bergmann and Tobias Tingberg, it has been very fun to share space, time, food, snacks, and stories with you. To have the chance to experience supervision has been very great for me. I am thankful for the pleasant processing times in the cleanroom together with Filip Hjort, Stefan Carlsson, Rickard Andersson, and Marcus Johansson, and I am grateful to them for their efforts which have in one way or another contributed to my work as well. I also thank Dr. David Adolph for sharing his nice and wise views regarding PhD studies. You David are a very good colleague.

I acknowledge the contributions from our collaborators in Prof. Grandjean's group at EPFL in Switzerland and Prof. Goano in Politecnico di Torino, especially Georg Rossbach and Marco Calciati for our joint publications. Many thanks also to my colleagues at Chalmers Dr. Martin Stattin, Dr. David Adolph, and Dr. Tommy Ive for providing the epitaxial DBR growth in our joint publications.

My great teachers especially at highschool Mr. Mohammadreza Tavajjoh and Mr. Babaei deserve a great deal of appreciation, as well as my professors during my bachelor's studies at Amirkabir University in Tehran, particularly Mr. Amir Kashi, Dr. Hassan Kaatuzian, and Dr. Mohammad Yavari. They were among the ones who gave me confidence and encouraged me to pursue my studies to a PhD level in europe.

Last but not least, I feel extremely lucky to receive so much care and love from my family. There are no words that can properly express my gratitude to love of my life, my dear wife, Pardis. Thank you for your love, warm support, and understanding through hardships. I am and will always be indebted to my wonderful mom and dad, Parvin and Mohammad for their genuine support and for believing in me. My dearest brothers Puyan and Kian deserve special thanks for always being there for me. I cannot wait to see you guys again and spend time with you all together. Very big thanks go to my supportive and kindhearted brother/sister-in-law Payam and Parand in Göteborg as well as Faramarz, Damon, and Babak. You have been one of the main reasons that I feel Göteborg like home. I want to thank all my family in Iran in particular Pegah, Meymanat, and Hemmat for being positive and their good wishes.

Financial support from the Swedish Research Council (VR), the Swedish Foundation for Strategic Research (SSF), the Swedish Energy Agency, the Department of Microtechnology and Nanoscience at Chalmers University of Technology, and the Hasselblad Foundation are acknowledged. The awarded travel scholarships from Chalmersska forskningsfonden and ÅForsk are also acknowledged.

Seyed Ehsan Hashemi

Göteborg
December 2016

Table of Contents

Abstract **i**

List of Papers **iii**

Acknowledgement **v**

1 Introduction **1**
1.1 Applications . . . 2
1.2 Scope and outline of thesis . . . 3

2 III-nitride material properties **5**
2.1 Crystal structure and features . . . 5
2.2 Origin of internal polarization fields . . . 5
2.3 Optical properties of III-nitride compounds . . . 6
2.4 Electrical properties . . . 8

3 III-nitride VCSELs **9**
3.1 GaN-VCSELs: state-of-the-art results and technologies . . . 10
3.1.1 Hybrid DBR design . . . 11
3.1.2 Double dielectric DBR design . . . 14
3.2 Additional challenges to be addressed . . . 15
3.2.1 Long or short cavity length . . . 15
3.2.2 Carrier leakage across active region . . . 16
3.2.3 Optical gain . . . 17
3.2.4 Transparent contacts . . . 17
3.2.5 Defects . . . 18
3.2.6 Temperature effects . . . 19
3.2.7 Lateral current and optical confinement schemes . . . 19

4 Guiding/Antiguiding effects in GaN VCSELs **21**
4.1 Intuitive picture of the structural sensitivity of guiding . . . 22
4.2 Optical guiding study . . . 23
4.2.1 Hot-cavity: The effect of self-heating . . . 25

4.3 The main conclusions 28

5 Electrically conductive epitaxial III-nitride DBRs 29
5.1 GaN-based DBRs 29
5.2 Mitigation of strain in AlN/GaN DBRs 30
5.3 Electrically conductive GaN-based DBRs 30
5.4 Electrical characterization of the n-type AlN/GaN DBRs 31
5.5 The main findings of the study 34

6 High contrast grating reflectors for GaN VCSELs 35
6.1 Structural description 36
6.2 HCGs as broadband reflectors for VCSELs 36
6.3 Fabrication of TiO_2/air HCG 38
6.4 Characterization of TiO_2/air HCG 42

7 Outlook and future directions 45

8 Summary of Papers 49

References 53

List of Acronyms 69

Papers A–E 71

Chapter 1

Introduction

There are two major types of semiconductor devices, the vertical-cavity surface-emitting laser (VCSEL) and the edge emitting laser (EEL). In VCSELs the beam emission is perpendicular to the plane of the epitaxial layers, while EELs emit through the cleaved facets perpendicular to the plane of the epitaxial layers. A VCSEL has a short cavity length (few 100's of nm to $\sim$1 μm), which results in a small active volume and thus ultralow threshold currents and single longitudinal mode characteristics [1]. The injected carriers and generated photons are strongly confined to small volumes both vertically and horizontally, leading to efficient and high modulation speed at low drive currents [2]. The VCSEL provides a circular symmetric low-divergent output beam which is suitable for coupling to multimode optical fibers. The possibility of on-wafer testing before separating and mounting the lasers results in low-cost production. VCSELs are also very suitable for formation of densely packed two-dimensional (2D) laser arrays [3].

The VCSELs are known since 1977, when Professor Kenichi Iga from Tokyo Institute of Technology established the concept and practically realized this new type of semiconductor laser [4, 5], which has over the years become the backbone light source of our data networks. In earlier research by Ivars Melngailis in 1965 [6], lasing parallel to the current injection was achieved for the first time. nowadays, the standard VCSELs emitting at infrared wavelengths (850 nm and even 980 nm) are now fully mature devices, and every year they are produced in millions. A key enabler has been the nearly lattice-matched AlGaAs material system, which is well-suited for monolithic growth of the multilayer VCSEL structure. The success of GaAs-based VCSELs has tempted both academia and industry to expand the emission wavelength range towards shorter and longer wavelengths. Unfortunately, the material systems required to achieve this are not as favorable.

VCSELs emitting in the visible regime are of high interest for many applications but require a completely different class of materials with large direct bandgaps. The

growth of high quality (low defect density) multilayer structures in those materials, is much more challenging, at least with today's technologies. The three main types of wide bandgap semiconductor materials are the group II-chalcogenides such as zinc-selenide (ZnSe), the group II-oxides such as zinc-oxide (ZnO), and the group III-nitrides such as gallium-nitride (GaN) [7]. In the II-VI material system, an electrically injected VCSEL emitting at 484 nm has been demonstrated at 77 K [8]. However, a major difficulty with the II-chalcogenides is the degradation under current injection. The II-oxides on the other hand suffer from the challenge of achieving high p-type doping levels. Today, the III-nitrides are the dominating material system. This thanks to the revolutionary work in the late 80's and early 90's to achieve p-type GaN and high power light emitting devices [9, 10]. Work that in 2014 was awarded with the Nobel prize in physics.

1.1 Applications

There is a need for compact, efficient, and low cost light emitters in the visible wavelength regime, where they will also enable new applications [11–16].

For example, in visible light communication (VLC) one can make use of the unregulated bandwidth of the electromagnetic spectrum to send and receive data in free-space, or underwater, with no interference and high security [17, 18]. GaN-based laser based light sources can enable efficient and high speed communication links thanks to their larger bandwidth and fast frequency response compared to the micro-light emitting diode (LED) systems that have so far been used in state-of-the-art VLCs [19, 20]. GaN-based edge-emitting lasers have been used to transmit 4 Gbit/s in a 0.15 m free-space link [21] and more advanced modulation schemes have been applied to reach 9 Gbit/s over 5 m in free-space [22]. A VCSEL could offer additional advantages compared to an edge-emitting laser, as mentioned above [23].

In solid-state-lighting (SSL) [24, 25], white light illumination is usually obtained using phosphor to convert part of the blue light from an LED into the other parts of the visible spectrum to achieve overall white emission. However, blue LEDs suffer from efficiency droop; a reduction of the radiative recombination efficiency at high current densities due to Auger recombination [26]. Hence to keep the efficiently high while generating enough lumens, a bulb must contain many LEDs inside, where each LED is operated at a low current density ($<$10 A/cm^2). This leads to lower lumen per LED chip area, which directly result in higher cost. In contrast to LEDs, laser devices operate under stimulated emission above threshold and therefore the Auger process is clamped at threshold. A high-power conversion efficiency (higher lumens) could be achieved at much higher current densities for the same chip size, resulting potentially in a higher output power and lower cost for laser-based lighting systems [27, 28]. VCSEL based SSL can offer a more directional and circularly-symmetric output beam with lower cost and little power consumption. Smart lighting systems can be designed with dynamic emission patterns by controlling individual lasers in a two-dimensional VCSEL array. In addition, a white VCSEL-based light sources could increase the functionality by an illumination source and a VLC [17, 29].

Red-green-blue (RGB) GaN-VCSELs could also be of interest for full-color laser display applications, such as head-up and near-eye displays [30], and picoprojectors [31], which do not require too high optical output power and where a low power consumption is a key factor [32]. By using lasers in these applications, higher resolution, higher brightness, and more compact carry-on devices can be obtained.

In bio-sensors and medical diagnosis and treatment, the interest for visible short wavelength lasers in the range of 400–500 nm is rapidly growing. Some of the examples include chemical tracking and biological agent detection based on exciting the dye molecule fluorescein around 494 nm and study the fluorescence [11, 33]. In optogenetics, stem cells can be genetically modified to render them sensitive to blue light; thereby, events in specific cells of living tissue can be controlled, with applications in artificial ears or eyes. Blue resonant light-emitters could enable novel designs and facilitate system integration into the body. In medical diagnosis, skin and esophagus cancer detection have become possible, without the use of biopsy, by using laser-induced fluorescence at a wavelength of 410 nm [34, 35]. This non-invasive technique is fast, reliable and reduces both pain and recovery time for the patient. Many of those applications would be interesting to integrate in a lab-on-chip, where the 2D array capability of the VCSEL would offer additional advantages [36].

These are only a few of the many applications for ultraviolet-blue-green VCSELs that can be foreseen, and many more will appear once such light sources actually exist.

1.2 Scope and outline of thesis

This thesis is devoted to GaN-based VCSELs. Chapter two presents some of the important material properties of the group III-nitride semiconductors. The state-of-the-art of electrically injected GaN-based VCSELs is summarized in Chapter three with a comparison between the competing technologies. In addition, some of the remaining challenges related to achieving better performing devices are introduced. In Chapter four, our work on how current aperture schemes can dramatically change the optical guiding, and thus the threshold current, is presented. Chapter five focuses on the effect of strain-compensating interlayers on the electrical conductivity of AlN/GaN distributed Bragg reflectors (DBRs). In Chapter six, a new method to fabricate a top reflector for nitride VCSELs based on a titanium-dioxide (TiO_2)/air high contrast grating is demonstrated. At the end an outlook about the prospects of III-nitride based VCSELs is given.

Chapter 2

III-nitride material properties

2.1 Crystal structure and features

III-nitride semiconductors such as GaN, or more generally (Al, In, Ga)-N alloys, are polytypic, [37], and can have a wurtzite or zincblende crystal structure. The wurtzite structure is thermodynamically stable under ambient conditions and is therefore the most common polytype. The zincblende structure can be stabilized by epitaxial growth of thin films on specific crystal planes of cubic substrates such as Si [38], SiC [39], and GaAs [40].

The zincblende structure has a cubic unit cell with a crystal structure identical to that of diamond (two interpenetrating face-centered cubic sublattices with an offset of one-quarter of distance along a body diagonal). Wurtzite, the more important polytype of III-nitrides, has on the other hand a hexagonal unit cell and thus two lattice constants, c and a. The crystal structure, which is shown in a stick and ball representation in Fig. 2.1, is formed by two interpenetrating hexagonal close-packed (hcp) sublattices, each with one type of atom, displaced with an offset of $\frac{5}{8}c$ along the c-axis. Therefore it can be identified by alternating biatomic close-packed (0001) planes of Ga and N pairs [37]. The three most important crystal planes are: (0001) the c-plane, $(1\bar{1}00)$ the m-plane, and $(11\bar{2}0)$ the a-plane, as illustrated in Fig. 2.1.

2.2 Origin of internal polarization fields

The wurtzite crystal is non-centrosymmetric. Due to the lack of an inversion symmetry plane and the difference in the electronegativity of the different atoms, the crystal is polar along the c-axis, resulting in Ga polar and N polar orientations [41]. This polarity leads to strong polarization fields in polar III-nitride semiconductors along the c-axis, both spontaneous and strain-induced piezoelectric polarization fields.

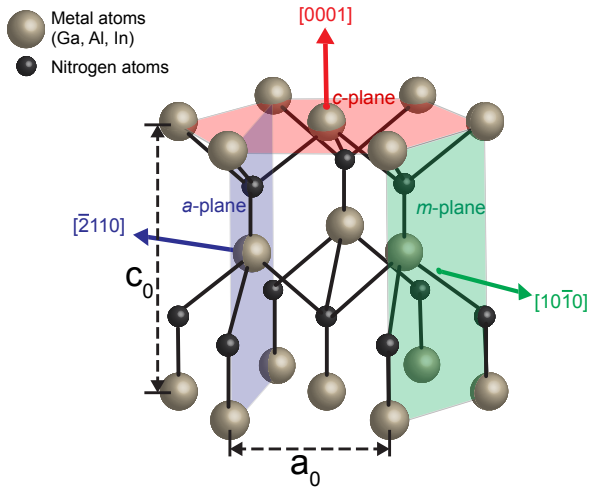

Figure 2.1: A stick and ball representation of the wurtzite crystal unit cell with Ga, Al, or In polarity, i.e., GaN (0001).

Even in an ideal wurtzite structure a non-vanishing spontaneous polarization is present due to the difference in electronegativity (electron cloud being closer to the nitrogen atoms). If the crystal is strained along the (0001)-plane, due to the difference between the lattice parameters or the thermal expansion coefficients in the hetero-structure, the piezoelectric effect can induce a polarization field. Therefore the piezoelectric polarization field is different depending on the type of the strain being tensile or compressive. The direction of the piezoelectric polarization field is presented in Fig. 2.2 for a Ga polarity with an in-plane compressive strain. The details of both types of polarization fields are discussed in refs. [37, 42].

The polarization fields are important to consider since they affect both optical and electrical properties of the materials.

2.3 Optical properties of III-nitride compounds

The wurtzite crystal structure of GaN, AlN, and InN offers an alloy system where the direct bandgaps can be tuned from 0.7 to 6 eV, corresponding to the emission wavelengths from infrared (1.7 μm) to ultraviolet (210 nm), see Fig. 2.3. A challenge however for hetero-structures in III-nitride-based materials is the large lattice mismatch between different compounds. As seen in Fig. 2.3 it is only ternary AlInN with 18% In composition that is lattice matched to GaN. There is also a lack of high quality, low cost substrates to grow III-nitrides on. In this figure, the most commonly used substrates are shown, except sapphire which has a lattice constant of a_0=4.765 Å, which falls outside of the graph.

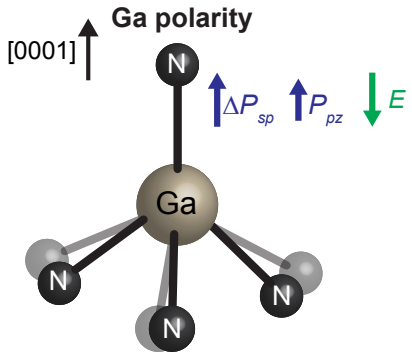

Figure 2.2: A tetrahedron with Ga polarity is shown in two different situations; without strain (light gray) and with compressive strain applied (black) in the c-plane.

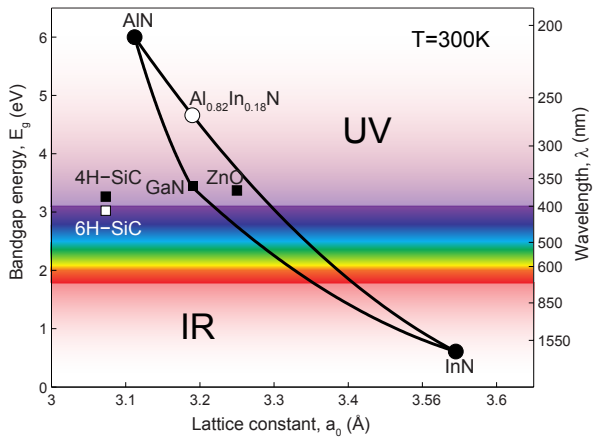

Figure 2.3: Room temperature bandgap of wurtzite III-nitride compounds versus the basal plane lattice constant a_0. The square markers represent the important substrates.

Furthermore, the III-nitrides are uniaxially optically birefringent, due to the polarity of the wurtzite crystal along the c-axis and anisotropy of the band structures resulting in anisotropic complex refractive index [43–45].

The internal electric fields, in the order of 10 MV/cm that arise from the polarization fields in polar materials are large enough to separate the electron and holes towards opposite sides of a quantum-well (QW), as illustrated in Fig. 2.4. This effect, known as the Quantum Confined Stark Effect (QCSE), leads to a reduction of photon emission rate as the overlap between the electron and hole wave functions is

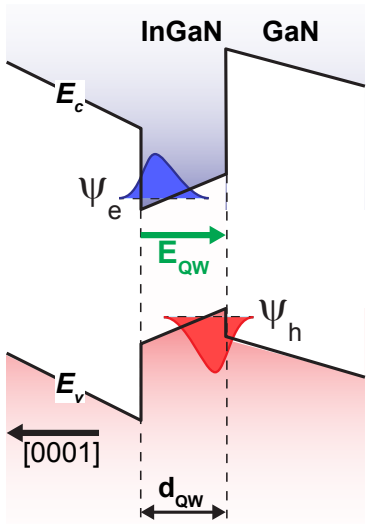

Figure 2.4: Energy band diagram of a c-plane InGaN QW with GaN barriers. Due to quantum confined Stark effect (QCSE) the overlap between the electron (Ψ_e) and hole (Ψ_h) wave functions is reduced. E_c and E_v are the conduction and valence band edge, respectively.

reduced and also to a red shift in the photoluminescence peak [46–48]. However at high injection current densities, typical for laser operation, these internal fields can be screened by the injected carriers [49].

2.4 Electrical properties

As-grown undoped GaN has typically a large unintentional background electron concentration of about 10^{16} cm^{-3}, which is attributed to the formation of nitrogen vacancies or unintentional incorporation of oxygen impurities in the lattice, acting like donors [50]. Intentional n-type doping is often done by incorporation of Si impurities, which have a fairly low ionization energy of 20 meV [51], resulting in most donors being ionized at room temperature. Typical electron mobility values lie in the order of 500 cm^{2}V^{-1}s^{-1} at room temperature. On the other hand, p-type doping of GaN is reputedly very challenging. Mg impurities are often used as acceptors to dope the GaN but their rather high ionization energy of 170 meV [52] leads to only a partial ionization of typically a few percent at room temperature. Moreover, the background electron concentration lowers the actual hole concentration, and hinders high p-doping levels. The difficulty to p-dope GaN is a major problem for most optoelectronic devices.

Chapter 3

III-nitride VCSELs

The attractive properties of VCSELs that were discussed in Chapter 1 are the main driving forces for the development of these devices also in the III-nitride material system. Looking at the history of GaN-based light emitters, major breakthroughs came in 1989 when Hiroshi Amano et al. [9] showed p-type conductivity in Mg-doped GaN material, which led to the first demonstration of high power GaN LEDs in 1991 by Shuji Nakamura [10]. In 1996 Nakamura also demonstrated the first continuous-wave (CW) operation of a GaN-based edge emitting laser diode at room-temperature (RT) [53]. Already in 1999 Nichia Corp. commercialized their first prototypes of GaN based edge emitting laser diodes. Soon lasers emitting at the wavelength of 405 nm with optical output power of several hundreds of milliwatts and lifetime over ten thousand hours were available from multiple commercial venders. As a result, the first Blu-ray optical data storage system was introduced in 2004 using InGaN laser diodes emitting at 405 nm [54].

The progress in III-nitride VCSELs has however been much slower, starting with a few sporadic demonstrations of lasing under optical pumping [55, 56] in addition to a few simulation reports proposing different structures for nitride VCSELs [57, 58]. In 2008, in separate works, researchers from National Chiao Tung University (NCTU) in Taiwan, first, and Nichia Corp. in Japan, second, finally showed the two first electrically injected GaN-VCSELs under CW operation at 77 K [59] and at RT [60], respectively. The long time span between the GaN edge emitting laser and the VCSEL shows that the GaN technology was not mature and developed enough to meet the tough requirements of VCSELs. Improvements in threshold current density, optical output power, and lifetime of today's III-nitride VCSELs are required before they can be of any real practical and commercial importance. To develop GaN-based VCSELs the focus should first be to minimize the optical losses in the cavity so that a high quality factor cavity (Q) and a low threshold current density can be achieved. The sources of the optical losses in the VCSEL cavity are usually a

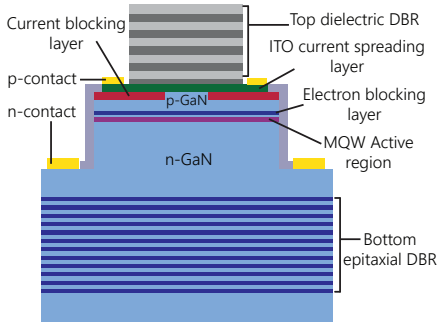

Figure 3.1: GaN VCSEL structure in a hybrid DBR scheme.

low reflectivity DBR, optical absorption, scattering losses due to inhomogeneities, etc. Furthermore, it is crucial to also address the hot-cavity properties at high operating injection current density, where self-heating can lead to higher losses due to temperature dependent material properties. The temperature effects have to be accounted for to be able to obtain a CW operation at elevated ambient temperatures, higher peak optical output power, and a longer lifetime.

This chapter will start with a summary and comparison of the cutting-edge technologies used in electrically injected devices by different groups, followed by a discussion on the major challenges in GaN-based VCSELs. The chapter will end by highlighting some additional challenges that still need to be addressed in future VCSELs.

3.1 GaN-VCSELs: state-of-the-art results and technologies

Figures 3.1 and 3.2 illustrate the two different device concepts that have been used for electrically injected GaN VCSELs. Either a hybrid DBR scheme has been used, i.e., a top dielectric DBR combined with a bottom III-nitride-based epitaxial DBR [61–63], or a double dielectric scheme using both a top and a bottom dielectric DBR [64–68]. The two DBR approaches are outlined in more detail in Section 3.1.1 and 3.1.2. All DBRs used so far in GaN VCSELs have been electrically insulating (except one recent report from Meijo University [69]). Thus, intracavity contacts are required together with long cavity lengths to reduce the lateral resistance. Another special feature with the GaN VCSEL is the use of a transparent current spreading layer (usually indium-tin-oxide, ITO) between the p-GaN and the dielectric DBR. This is required to spread the current laterally since p-GaN has a low electrical conductivity. The current is confined to the center by using a dielectric aperture in most cases. Table. 3.1 summarized available details of the electrically injected VCSEL structures published so far. All structures are grown on c-plane except the structures made by UCSB which are grown on the non-polar m-plane. As can be seen in the table, there

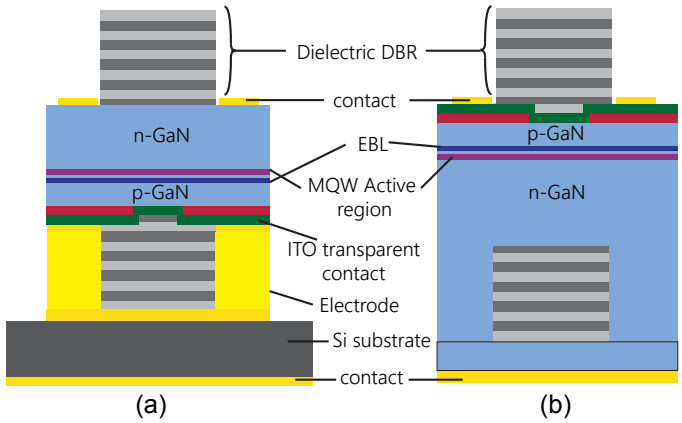

Figure 3.2: GaN VCSEL structures in double dielectric DBR scheme using, (a) substrate removal approach, (b) epitaxial lateral overgrowth approach.

is not much consensus on which is the best structure for a GaN VCSEL, indicating that GaN VCSELs are still in the early stage of their development.

The performance characteristics of the published devices, in terms of output power and threshold current density are plotted in Fig. 3.3. To be able to compare results with different aperture sizes, current density is plotted instead of current. However, it is important to note that in most of these published GaN-VCSELs the emission profile across the whole aperture is not very uniform due to inhomogeneous current injection and filamentary lasing. As seen in Fig. 3.3, there are now several reports with milliwatt class optical output power and decent current densities, where the best performance characteristics have been presented by National Chiao Tung University [70] in Taiwan, and Meijo University [71], Sony [72], and Nichia [64] in Japan.

Two of the major issues in VCSEL design is to ensure a spatial alignment between the standing optical fields and the thin active region (i.e., the peak of the standing optical field has to be well-aligned to the position of the QWs), and also a spectral matching between the material gain spectrum of the active region, the reflectance spectrum of the mirrors, and the resonance wavelength of the cavity. Both the hybrid DBR and double dielectric DBR schemes have some advantages and disadvantages with regard to these spatial and spectral alignment requirements, which will be further discussed in the following sections.

3.1.1 Hybrid DBR design

High reflectivity, broadband epitaxial mirrors are not easy to achieve in the III-nitride material system due to a lack of two lattice matched materials with large refractive index difference. Two approaches have mainly been explored, Al(Ga)N/(Al)GaN and AlInN/GaN. AlGaN DBRs offer high refractive index contrast if the binary material

Table 3.1: Different approaches and structures used in electrically injected GaN VCSELs [59–79].

	NCTU 2008 **(2010)**	Nichia 2008	Nichia 2009 **(2011)**	Panasonic 2012	EPFL 2012	UCSB 2012	Xiamen 2014	NCTU 2014 **(2015)**	Sony 2015 **(2016)**	UCSB 2015 **(2016)**	UCSB 2015	Meijo 2016 **(2016)**	Meijo 2016
Top DBR	8× **(10×)** Ta_2O_5/ SiO_2	7× Nb_2O_5/ SiO_2		ZrO_2/ SiO_2	7 × TiO_2/ SiO_2	13× Ta_2O_5/ SiO_2	14× ZrO_2/ SiO_2	10 × Ta_2O_5/ SiO_2	12× (11.5×) Ta_2O_5/ SiO_2	16× Ta_2O_5/ SiO_2	16× Ta_2O_5/ SiO_2	8 × Nb_2O_5/ SiO_2	8 × Nb_2O_5/ SiO_2
Current spreading layer	240nm ITO **(30nm ITO and 2nm p+ InGaN)**	50 nm ITO		100 nm ITO	50 nm ITO	50 nm ITO	30 nm ITO and 2nm n-InGaN	40 nm annealed ITO	30 nm ITO	47 nm ITO	141 nm TJ consisting n++GaN/n-GaN/n++GaN/n-GaN [39.6/39.6/39.6/22.1] nm	20 nm ITO	20 nm ITO
P-GaN thickness	120nm **(110nm)**				97 nm p-GaN and 20nm p+ GaN	113 nm p-GaN and 14nm p++ GaN	159 nm	100 nm	∼100 nm	56 nm	62.2nm p-GaN +14nm p++ GaN	60nm p-GaN +10nm p+ GaN	60nm p-GaN +10nm p+ GaN
Aperture	200nm SiN_x	SiO_2	SiO_2	SiO_2	Plasma passivated p-GaN surface	SiN_x	SiO_2	200nm SiN_x	SiO_2 (Boron implantation)	Al ion implantation **(airgap)**	Al ion implantation	SiO_2	SiO_2
Aperture diameter	10µm	8µm	8µm **(10µm)**	20µm	8µm	7µm	10µm	10 µm **(5µm)**	8µm	12µm	12µm	8µm	8µm
EBL	– **(24nm AlGaN)**	–	–	p-AlGaN	20nm p-AlGaN	15nm p-AlGaN	20nm p-AlGaN	Composition graded Al_xGaN **(AlGaN/GaN multiple quantum barrier)**		5nm p-AlGaN	5nm p-AlGaN	20nm p-AlGaN **(15nm p-AlGaN)**	20nm p-AlGaN
QWs / Barriers	10× InGaN/ GaN [2.5 nm/ 7.5nm] **([2.5nm/ 12.5nm])**	2× InGaN/ GaN [9nm/ 13nm]	5×		5× $In_{0.10}GaN$/ $In_{0.01}GaN$ [5nm/5nm]	5× $In_{0.12}GaN$/ GaN [7nm/5nm]	5× Coupled InGaN/ GaN [4nm/ 4nm]	10× $In_{0.1}GaN$/ GaN [2.5nm/ 10nm] **(5× $In_{0.15}GaN$/ $In_{0.02}GaN$ [4nm/8nm])**	2× (4×) InGaN/ GaN [6nm/ 10nm]	7× InGaN/ GaN [3nm/1nm]	7× InGaN/ GaN [3nm/1nm]	Two 5× 3 nm InGaN/ 6 nm GaN MQWs +45 nm p-type intermediate layer **(5× 6 nm InGaN/ GaN MQWs)**	5× InGaN/ GaN MQWs [3nm/6nm]
n-GaN thickness	790nm **(860nm)**				944nm	902nm		880nm	4µm ELO	50nm n++ and ∼770nm n-GaN	762nm	400 nm **(300 nm)**	50 nm
Cavity length	$5\lambda^*$ **($7\lambda^*$)**	$7\lambda^*$	$\sim 20\lambda^*$	35λ	$7\lambda^*$	7.5λ	$\sim 13\lambda$		$20\lambda^*$	6.95λ		$4\lambda^*$	$1.5\lambda^*$
Bottom DBR	29× AlN/GaN with SPSL	11× SiO_2/ Nb_2O_5	11× SiO_2/ Nb_2O_5	SiO_2/ ZrO_2	42× $Al_{0.82}InN$/ GaN	13× SiO_2/ Ta_2O_5	17.5× SiO_2/ ZrO_2	25× AlN/ GaN	14.5× SiO_2/ SiN_x	10× Ta_2O_5/ SiO_2	12× Ta_2O_5/ SiO_2	40× AlInN/ GaN	Si-doped 46× AlInN/ GaN
Substrate	Sapphire	Sapphire	FS-GaN	FS-GaN	FS-GaN	FS-GaN m-plane	Sapphire	Sapphire **(GaN)**	GaN	FS-GaN m-plane	FS-GaN m-plane	FS-GaN	FS-GaN
Substrate removal technique	–	LLO and CMP	CMP	CMP	–	PEC	LLO, ICP, and CMP	–	Lapped to 80µm and packaged	PEC	PEC	–	–

* The penetration depth into the DBR is not accounted for.

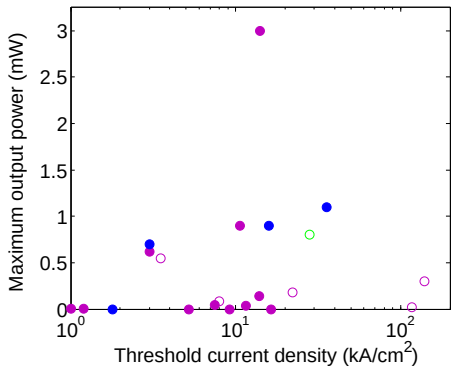

Figure 3.3: Optical output power and current density of electrically injected GaN-VCSELs published to date [59–79]. Filled markers illustrate CW operation and open markers are pulsed operation. The colors indicate the lasing wavelength, violet (405–422 nm), blue (446–463 nm), and green (503 nm). The markers shown at zero output power denote the reports where the output power is only given in arbitrary units.

compounds AlN/GaN are used, see Table 3.2, but suffer from large difference in in-plane lattice constant of ∼2.5%. Strain compensating structures are therefore included in the DBR to minimize crack formation. AlInN/GaN is lattice matched if the In composition is near 18%, but offer a much lower refractive index contrast and such a DBR therefore require many more DBR pairs to achieve high reflectivity and thus results in a narrowband reflectivity.

Three groups have so far been able to grow high quality nitride-based DBRs and therefore have taken the hybrid DBR approach: National Chiao Tung University (NCTU) in Taiwan with an AlN/GaN DBR [80], EPFL in Switzerland with an AlInN/GaN DBR [81], and Meijo university in Japan with undoped and doped AlInN/GaN DBRs [63, 69]. The AlN/GaN option required special structures to reduce the tensile stress, a short-period superlattice (SPSL) of AlN/GaN was placed after every fifth DBR period for the first 20 pairs and after every third DBR period for the last 9 pairs. This DBR showed a peak reflectivity of 99.4% and a full width at half maximum (FWHM) of 25 nm. Gatien Cosendey and coworkers at EPFL took a lattice-matched approach using a combination of $Al_{0.82}In_{0.18}N$ and GaN for their bottom DBR. The relatively low refractive index contrast between these two compounds requires a large number of at least 46 mirror pairs in the DBR for a wavelength of 420 nm and 54 mirror pairs for a wavelength of 450 nm. The EPFL team has demonstrated peak reflectivity of 99.6% with a stopband width of 26 nm [81] and the Meijo group has been able to obtain a peak reflectivity of 99.7% at a wavelength of 410 nm [71]. The top DBR in the hybrid design is made of dielectric materials and therefore a 99.9% reflectivity with a broad stopband can easily be achieved thanks to the high refractive index contrast between the dielectric materials. In the hybrid DBR design, it is most likely that the epitaxial nitride-based DBR has a lower peak

reflectivity than the dielectric DBR, and therefore it is most suited for bottom emitting configuration. This has been observed from a VCSEL by the Meijo group where 3 mW of optical output power was achieved from the bottom epitaxial DBR, while the optical output power from the dielectric DBR side was five times lower [71].

Table 3.2: Material data at room temperature.

Material	Refractive index at 420 nm	Lattice constant, a_0 (Å)
AlN	2.18	3.112
$Al_{0.82}In_{0.18}N$	2.3	3.189
GaN	2.49	3.189

3.1.2 Double dielectric DBR design

The challenges with the epitaxial growth of high quality III-nitride DBRs have stimulated the development of the double dielectric DBR scheme. With dielectric materials lattice matching is not a prerequisite. In addition, a large refractive index contrast (44% if SiO_2/TiO_2 used) can be achieved which results in very broadband reflectivities. This is very favorable for GaN VCSELs which require a good matching between the peak reflectivity, optical gain, and the resonance wavelength, something not easy to achieve for a cavity length of about 1μm, see Section 3.2.

two main approaches have so far been proposed to incorporate dielectric DBRs on both sides of the VCSEL cavity in the double dielectric DBR scheme, see Fig. 3.2. In one approach the growth substrate is removed to deposit a second dielectric DBR on the bottom of the n-GaN contact layer, where a prior flipchip bonding is required to provide a supporting substrate while handling the thin epi layers after the substrate removal. Second approach relies on an epitaxial lateral overgrowth (ELO) technique. In both techniques, maintaining a precise control of the cavity length can be challenging. To remove the growth substrate, different methods such as laser-induced lift-off (LLO), chemical and mechanical polishing (CMP), and bandgap-selective sacrificial photoelectrochemical etching (PEC) have been used. Among these, the PEC has by far been the most promising method providing accurate cavity length control by using a sacrificial etch stop layer. In the latest GaN VCSELs, the structures are often grown on free-standing (FS) GaN substrates for higher structural quality. In these cases, the LLO method could not be easily applied as there is no light absorption contrast between epitaxial GaN and the GaN substrate for the heat generation and material decomposition. To use CMP technique to thin-down the FS-GaN substrates is not preferred since the hardness of GaN materials easily leads to large thickness variation across a large-area substrate. In the ELOG method, no substrate removal/bonding is necessary but the growth needs to be optimized so that the desired ratio between the vertical and lateral growth rates can be achieved and precisely controlled.

An intrinsic challenge that remain with the double dielectric DBR scheme, is the poor heat dissipation capability since the III-nitride cavity is sandwiched between two DBRs with very low thermal conductivity. This can easily result in rapid temperature increase in the cavity close to the active region. To achieve CW operation can

therefore be challenging in the double dielectric DBR scheme. The problems regarding the temperature effects in GaN VCSELs are discussed further in Section. 3.2.6.

3.2 Additional challenges to be addressed

In order to improve the performance of GaN-VCSELs, a few remaining issues should be addressed besides the ones already mentioned in the previous sections.

3.2.1 Long or short cavity length

In most of the reported electrically injected GaN-VCSELs a cavity length of between 7λ to 20λ have been used, mainly due to $\sim 1\mu$m n-GaN layer thickness in the cavity. To shrink the n-GaN thickness there are several limitations which are explained as follows.

As discussed earlier, the GaN-VCSELs have been imposed to intracavity contacts due to the lack on conductive DBRs (undoped and dielectric). The use of intracavity contacts requires a not too thin n-GaN layer to keep the lateral resistance from the n-contact to the center of the VCSEL low. Moreover, in the double dielectric scheme, thicker n-GaN layers have been preferred in order to protect the delicate active region from the harsh substrate removal processes (such as LLO and CMP), and also to avoid possible stress fractures in the GaN film during the bonding process [82]. In addition, an alternative approach to trying to uphold the precise overlap between the gain spectrum, mirror reflectance spectrum, and cavity resonance wavelength is to make the VCSEL cavity longer to shrink the longitudinal mode spacing. For a long cavity, the many longitudinal modes ensure that at least some always overlap with the material gain, and even when the gain spectrum shifts due to temperature effects some modes will still be lasing. This is the approach taken by a group at Panasonic [65] who used a cavity length of about 35λ. Of course, the optical losses in long cavity design will most likely be larger and the threshold current to achieve lasing will thus not be the lowest possible. On the other hand, the threshold gain in a long cavity design is less sensitive to fluctuations in cavity length, which can be large in the case when CMP has been used to remove the substrate [83]. Finally, in the double dielectric scheme, a longer cavity can be beneficial. Increasing the thickness of the epi-layers beneath the dielectric DBR layer can improve the dissipation of the generated heat more efficiently ensuring lasing under CW operation at elevated ambient temperatures.

Since this layer is doped, the free carrier absorption, which is an optical loss process, can be overall high for a very thick n-GaN layer. The effect of n-GaN layer thickness on the device performance can be explored. Using the 2D effective index method explained in [84] we have calculated the threshold gain as a function of the absorption coefficient and n-GaN layer thickness, illustrated in Fig. 3.4a. Moreover, current transport simulations conducted by our partners at Politecnico di Torino show that the n-GaN thickness in a hybrid VCSEL mesa with intracavity contacts can be reduced to about 500 nm and still avoid a too high resistance, as shown in Fig. 3.4b.

Another drawback with using a $\sim 1\mu$m thick n-GaN layer is difficulty in controlling the absolute cavity length accurately. The effect of small variations in n-GaN thicknessfor a hybrid VCSEL with a 42-pair AlInN/GaN DBR is illustrated in Fig. 3.5, which shows that the thickness of the n-GaN layer has to be controlled to within ± 20 nm.

3.2.2 Carrier leakage across active region

Injected carriers should be confined both radially (to the center of the structure) and longitudinally (in the multiple QW layers). Apart from the radial carrier confinement, which will be discussed in Sec. 3.2.7, the longitudinal (vertical) carrier

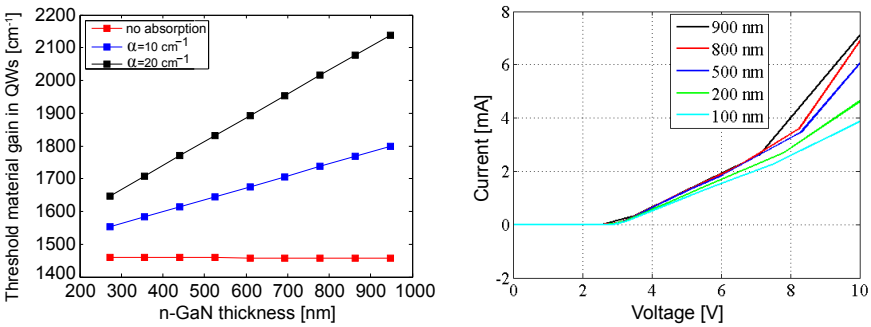

(a) (b)

Figure 3.4: (a) Threshold gain values for the same VCSEL structure with various n-GaN thicknesses with different assumptions on the free carrier absorption coefficient α of the n-GaN layer. (b) Current-voltage curves for a hybrid VCSEL mesa obtained from APSYS simulations, with various n-GaN thicknesses.

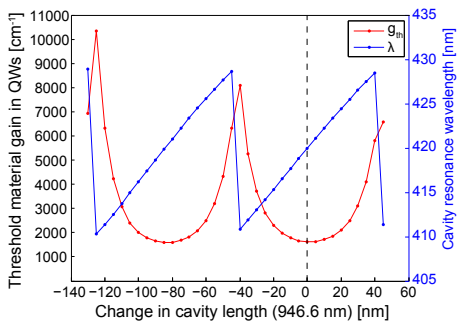

Figure 3.5: The effect on threshold gain and resonance wavelength of a small variation in the thickness of the n-GaN layer, assuming no optical absorption in the ITO.

injection/distribution among the multiple QWs can be problematic due to several issues such as the strong imbalance between electron and hole mobilities, large band offsets, and the internal polarization fields. In order to minimize a large carrier leakage across the active region, electron blocking layers (EBLs). They are realized by inserting extra potential barriers for electrons between the QWs and the p-GaN layer. An efficient EBL design, which can effectively hinder the electron leakage and not much affect the hole injection, seem to be very crucial to obtain higher radiative recombination rates in QWs and low threshold operation. Many different EBL designs have been tested and their effect on VCSEL performance have been studied such as p-doping of the EBL [85], compositionally graded EBL [86], and multiple barrier EBL [87]. The different EBL designs used in GaN VCLSLs are summarized in Table 3.1.

3.2.3 Optical gain

As can be seen in Table 3.1, the earliest reports on electrically injected GaN-VCSELs had a high number of QWs, maybe to achieve a maximum optical gain per round tip and increasing the overlap of the standing optical field with the gain region. However it was later shown that due to nonuniform carrier distribution across the multiple QWs, only the QWs which are closest to the p-GaN layer can be pumped above their transparency and contribute to the optical gain. The QWs on the n-side will then be absorbing, reducing the net gain [88, 89]. Higher optical gain can be obtained by growing on nonpolar or semipolar planes which can provide a better overlap between the electron and hole wavefunctions as the effects from the internal built-in polarization fields are much less or non-existing [74, 90].

3.2.4 Transparent contacts

In the beginning of this chapter, it was already discussed that transparent current spreading layers are necessary in GaN-VCSELs to minimize the current crowding due to the inefficient lateral current transport in the p-GaN layer. A high quality current spreading layer should ideally provide high transparency, high conductivity, and ohmic contact to p-GaN which can withstand high injection current densities used in GaN VCSELs. Indium-tin-oxide (ITO), in amorphous or poly crystalline forms, has so far been used in almost all of the realized GaN-VCSELs because of its high electrical conductivity and optical (semi-)transparency. The only exception is the incorporation of tunnel junction (TJ) in an m-plane GaN VCSEL published by UCSB [77]. Despite this wide usage, the properties of ITO are not ideal and has a direct negative impact on the device performance. ITO has an optical absorption coefficient of >1000 cm-1 at blue wavelength range, and there is even a trade-off between ITO transparency and its conductivity. Therefore, to minimize the optical absorption of the ITO layer, thickness $\sim$30 nm has often been used, and the layer should be placed in an optical field node of the VCSEL cavity. unfortunately, there is still a risk of increased optical absorption loss if the cavity length deviates from the design by a small margin.

ITO deposition, usually done by physical vapor deposition (PVD) techniques to achieve high quality [91], can lead to p-GaN plasma damage [92]. This sets a limitation to the maximum plasma power that should be used for ITO deposition which can lead to increased porosity (less quality) of the ITO film. If plasma damage occurs, the contact resistivity between the ITO and p-GaN will be very high which can worsen the current injection and increase the heat generation in the device and lead to break down of the device. Some companies have mastered the ITO deposition on p-GaN surfaces [93, 94]. Although they do not reveal their exact process strategies, it is likely that they make use of a multilayer ITO in which the first layers are more porous to avoid plasma passivation of the p-GaN layer, and the upper layers are more dense for their increased conductivity with a sheet resistance down to $\sim$15 Ω/sq. It is shown that a smooth ITO layer, preferably with a roughness(root-mean-square)$<$1 nm, is necessary to keep scattering losses low enough in the VCSEL [95].

Investigations on alternative solutions for an efficient current spreading layer for GaN VCSELs is still on going. Even though ITO might still be a reasonable candidate for GaN VCSELs in the visible spectral range, but its optical absorption loss in the ultraviolet (UV) regime is highly increased [96]. There have been many attempts to realize other types of transparent current spreading layers such as graphene (2D materials) [97], Al-doped ZnO [98], thin metal films [99, 100], etc, mainly in GaN-based LEDs. Thin metal layers have a trade-off between low sheet resistance, low resistive contacts to p-GaN, and a low optical absorption [101]. In addition, high quality, single layer graphene has been transferred to p-GaN, showing 97.7% transmittance in the visible wavelength range. As a result of the high contact resistivity the transferred graphene did not withstand high injection currents [97, 102]. Recently, in order to improve the contact resistivity, there have been attempts to directly grow single or multilayer graphene on p-GaN [103, 104].

The most promising approach to date to replace ITO is the tunnel junction (TJ). TJs are a standard technology in InP-based VCSELs which share some of the challenges with GaN-based VCSELs [105]. By incorporation of a thin TJ structure, the top part of the GaN VCSEL structure, which usually consists of a p-type GaN layer and ITO, can be replaced by a much more conductive n-GaN layer. The n-GaN layer is not only less resistive but also less optically absorptive than the p-GaN and ITO. By suppressing the current crowding effect in the resistive p-GaN layer, there will be no need for a current spreading layer, such as ITO. The TJ can make the current transport much more efficient, with the expense of slightly adding to the overall series resistance of the device.

To conclude, so far ITO has shown the best performance in terms of electrical conductivity, contact resistance, and optical transparency. The research is still ongoing to find another material with better electrical and optical properties than ITO or to pursue a technological change in the structure so that a current spreading layer would not be needed anymore.

3.2.5 Defects

The high density of defects in the epitaxial III-nitride layers can limit the optical and electrical performance in VCSELs, for example by increasing the scattering loss.

Dislocations can form current leakage paths, making the realization of effective current injection much more challenging. In QWs, they can contribute to the increased rate of unwanted non-radiative recombination. So far in GaN based LEDs, grown on foreign substrates such as sapphire, high internal quantum efficiencies have been achieved despite the high dislocation density, which has been attributed to the localization effects, in which the dislocations sites are screened and have a reduced impact [106, 107]. However, for lasers it is still essential to decrease the dislocation density levels since the operating injection current densities are much higher in lasers. By using GaN substrates instead of sapphire, devices with better performance are therefore expected [73].

3.2.6 Temperature effects

In GaN-VCSELs, several factors such as a large contact resistivity (mainly between ITO and p-GaN) and the inefficient current transport properties (due to current crowding and carrier leakage, see Section 3.2.2) lead to an increased operating voltage and high injection current density for lasing. Thus, efficient heat dissipation is essential, otherwise the large resistive heat generation can degrade the device rapidly and prevent it from lasing under CW operation.

The short lifetime of today's GaN-VCSELs is mostly attributed to this excessive heat generation. The heating effects may not only modify the guiding properties of the cavity (see Chapter 4 and Paper C), but can also decrease the optical material gain in the QWs, as well as reducing the modal gain since the spectral overlap between the gain peak and the resonance change with temperature. Due to the temperature effects, the VCSEL can prematurely reach the thermal roll-over point, limiting the maximum achievable output power.

In the hybrid DBR scheme, heat dissipation can for example occur through the substrates to reduce the temperature rise. Devices grown on sapphire substrates, with poor thermal conductivity, may therefore not be preferred.

If a double dielectric scheme is used, the bottom dielectric DBR can be etched into a small diameter mesa and plated with metals to improve thermal dissipation [66, 67]. As it was discussed earlier in Section 3.2.1, a long cavity length could also be useful to more efficiently remove the heat from the central part of the cavity. In addition, long cavities will decrease the longitudinal mode spacing, allowing many modes to overlap with the optical gain spectrum, which makes the laser less sensitive to the temperature induced gain shift. In [65], a cavity length as long as 35λ has been used for this purpose. However the problem with reduced QW material gain at higher temperature still remains. Regarding this, the group at UCSB have never been able to show CW operation for their m-plane GaN-VCSELs, most probably due to poor thermal dissipation in their double dielectric structures.

3.2.7 Lateral current and optical confinement schemes

It is essential to confine both the current and the optical field laterally to the center of the VCSEL to increase the overlap between gain and optical field, and to be able to achieve the high threshold current densities required for lasing, typically 10

kA/cm^2. The confinement technique that is widely used in GaAs-based VCSELs, partial oxidation of a high Al-content layer, is not easily implemented in III-nitride-based materials. Therefore, many groups have formed an electrical aperture between the p-GaN and the ITO, mostly by using a low index dielectric material that blocks the current, and opening a hole in its center to pass the current through. However, this scheme results in a non-planar structure that is depressed in the center, i.e., has a downward step profile. We have investigated the optical properties of such cavities in terms of guiding properties and losses using our in-house developed VCSEL simulation tools that are based on the effective index method (EIM) and 3D coupled-cavity beam propagation method. We found that the non-planar centrally depressed structures yield an anti-guided cavity with associated high losses, see Chapter 4. To achieve GaN-VCSELs with low threshold currents such structures should be avoided.

Chapter 4

Guiding/Antiguiding effects in GaN VCSELs

Achieving a high enough current density to reach lasing obliges the introduction of an aperture to confine the current to the central part of the device. However, the intracavity aperture also manipulates the optical properties of the laser cavity, both because the cavity structure changes and because the confined current changes the refractive index profile, since it depends on both temperature and carrier distribution. It turns out that both structural and thermal modifications have a strong influence on the ability of the cavity to guide the light, i.e., to minimize radiation loss in the transverse direction. This chapter describes these effects, how they can be modeled, and the strong impact they can have on the laser performance.

Previously, current apertures in GaN-based light emitting devices had mainly been divided into three schemes: (1) dielectric SiN_x or SiO_2 apertures; (2) epitaxial AlN [108, 109] and AlInN [110] apertures using regrowth; (3) oxide apertures through selective oxidation of AlInN [111]. In schemes (1) and (2), the idea was to obtain a transverse current confinement by deposition of an electrically non-conducting layer and then making an opening (a few micrometer in diameter) in the center to pass the current through. The surface of the resulting structure was no longer planar but had a negative (downward) step profile, referred to as a "depression" in the structure, see Fig. 4.1. In scheme (3), a continuous AlInN layer was grown in between the p-GaN layers, which was then selectively oxidized from the mesa sides. In this case, the surface of the structure will be planar and flat, assuming the oxidation does not lead to strong expansion or contraction of the oxidized material.

Most of the reported GaN-based VCSELs before 2014 [59, 60, 65, 66, 74] have employed only scheme (1), probably due to the difficulty of controlling the oxidation and/or the regrowth processes in schemes (2) and (3). The only exception was the work by Cosendey and coworkers at EPFL [62], in which the transverse current confinement was obtained using p-GaN surface passivation by reactive ion etching (RIE) with an Ar/CHF_3 plasma. The RIE treatment slightly etched the material

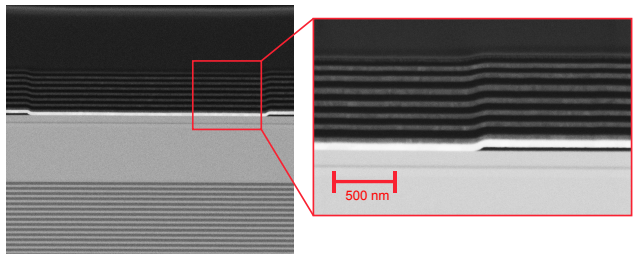

Figure 4.1: Central depression of the top surface in a device with a SiO_2 aperture.

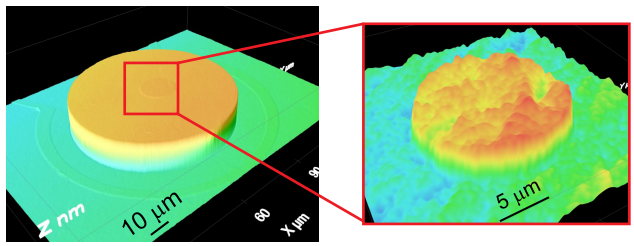

Figure 4.2: Central elevation of the top surface in the device with RIE-treated GaN.

outside the aperture region so that the top surface of the structure had a shallow elevation of about 10 nm in the center, shown in Fig. 4.2. As will be shown, the degree of depression or elevation of these non-planar structures is simply and directly related to the ability of the laser cavity to work as a good waveguide. This is of great importance for efficient operation of semiconductor lasers by providing a better overlap between the photons and the charge carriers and reducing excessive transverse radiation loss.

4.1 Intuitive picture of the structural sensitivity of guiding

Good guiding of the light, propagating in the laser cavity, is obtained when the so-called effective index of the structure at the center of the device is higher than that in the periphery. In the case of structures with depression in the center, the layers that are deposited after the formation of the aperture, e.g. ITO layer and dielectric DBR, will basically preserve this shape having a similar depression equal to the thickness of the aperture layer. However, in such non-planar multilayer structures there will be some cross-sections in which the refractive index of the material in the periphery is larger than that of the central part, as shown by the red dashed lines in Fig. 4.3. There is therefore a large risk that if the standing optical field is strong at these cross-sections, the overall device will act like an anti-guided structure. An

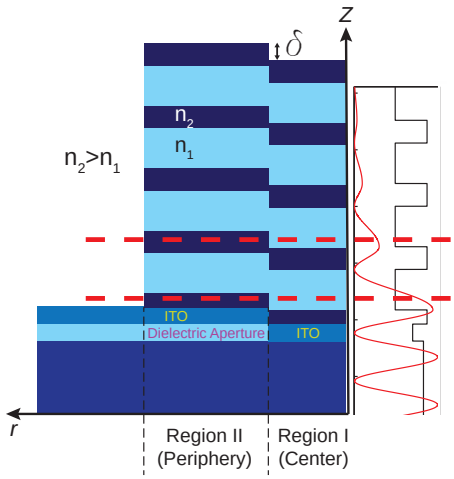

Figure 4.3: Schematic illustration of part of the VCSEL structure where the introduction of an aperture has resulted in a depression by δ in the central part. At the cross-sections shown by red dashed-lines the refractive index in the periphery is larger than in the center, which can possibly lead to antiguiding. Also shown is the refractive index profile at the center of the device and the amplitude of the optical field along the symmetry (z-)axis.

anti-guided structure will lead to a higher lateral radiation loss and thereby higher threshold currents and lower output powers, if lasing at all is possible.

4.2 Optical guiding study

In order to theoretically investigate the behavior of the cavities with different planar and non-planar structures, a numerical simulation model based on a quasi-2D effective index method (EIM) was applied to calculate the cold-cavity index guiding, Δn_{eff}, values [84]. The Δn_{eff} parameter depends on the cavity structure and the modal field distribution. It was found to be a very reliable indicator of the cavity's ability to guide the light and prevent lateral loss, as will be shown. The EIM can also provide accurate threshold gain values for every transverse mode if the structure is weakly positively index guided, i.e., $0<\Delta n_{eff}<0.03$. Under such conditions, the lateral radiation loss is negligible. In other cases, i.e. for strong positive guiding and negative guiding (anti-guiding), another model based on a three-dimensional (3D) Beam Propagation Method (BPM) was used. It requires a substantially longer computation time, but accounting for lateral radiation loss mechanisms including diffraction and lateral leakage, the latter which signifies the excessive lateral loss that occurs in antiguided cavities [112].

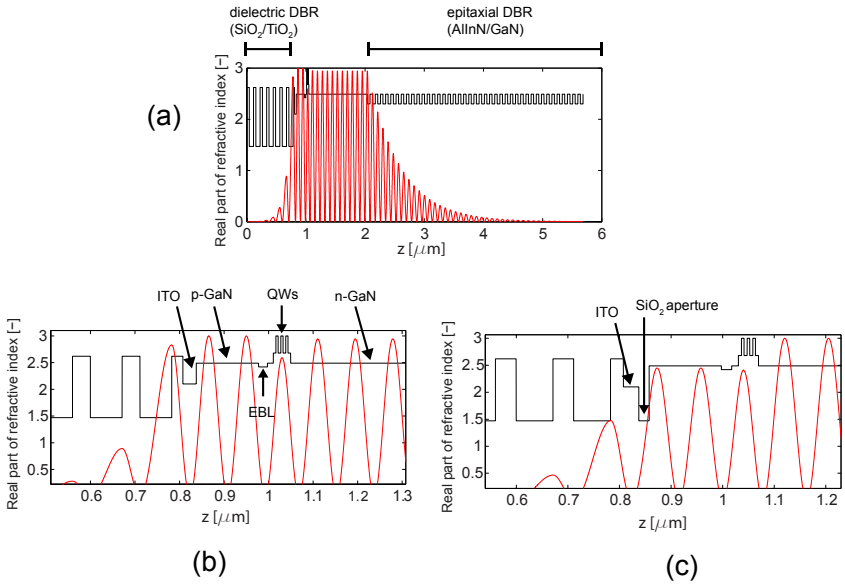

Figure 4.4: Longitudinal profiles of the refractive index (black) and standing optical field (red) calculated with EIM in a GaN-VCSEL structure. (a) Region I, which is the center of the device, (b) zoom-in of region I (c) zoom-in of region II, which is the periphery of the device. (Note the low-index SiO_2 aperture between the p-GaN and ITO.

Using the 2D-EIM model described in [84], the Δn_{eff} value is calculated by performing a 1D-simulation in the center of the structure and another one in the periphery (where the aperture is incorporated). From each of these runs, a list of different parameters is calculated: cavity resonance wavelength, λ_0, threshold material gain in QW, g_{th}, variation in the real part of the effective dielectric constant, $\Delta \mathrm{Re}(\epsilon_{eff})$, weighted dielectric constant, $\langle \epsilon \rangle$, and cavity quality factor, Q, among others. The index guiding value is then calculated as,

$$\Delta n_{eff} = \frac{\Delta Re(\epsilon_{eff})_{center} - \Delta Re(\epsilon_{eff})_{periphery}}{2 \times \sqrt{\langle \epsilon \rangle}}, \tag{4.1}$$

Figure 4.4 illustrates the standing optical fields that are obtained for a VCSEL structure in the two regions. Region I is the center of the device inside the aperture and region II is in the periphery of the device where a dielectric SiO_2 layer exists between the p-GaN and the ITO layers.

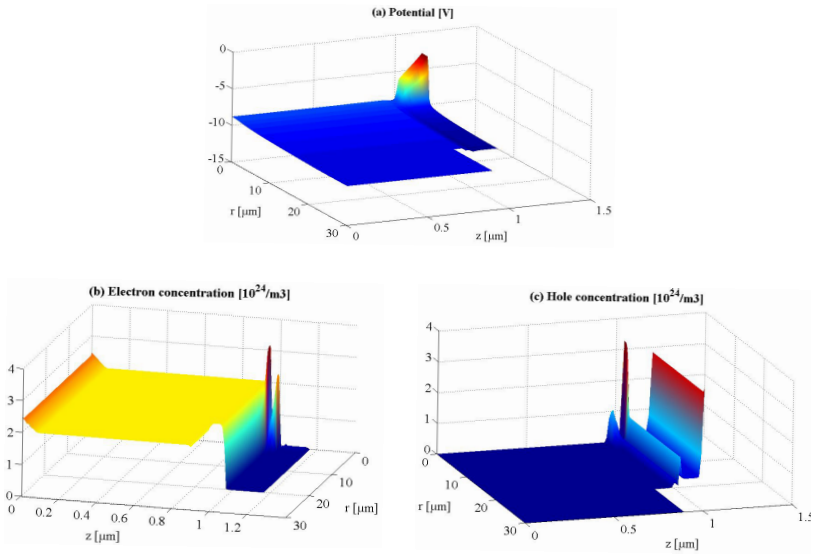

Figure 4.5: Current transport simulation results using APSYS software, under drive conditions of 10 V potential difference between p- and n- contacts corresponding to a total current ∼8 mA through a circular aperture with a 2 μm radius.

4.2.1 Hot-cavity: The effect of self-heating

A realistic investigation of GaN-based lasers under operation should in principle include the significant temperature rise inside the cavity. Large self-heating occurs in the cavity since the required injected current densities and the existing internal resistances are both high. Self-heating in semiconductor lasers can have a large impact on the optical properties of the device due to the temperature-induced change in the refractive index. Besides, the bandgap of semiconductors shrinks with increasing temperature. Therefore, it was well justified to extend the previous simulations by including the temperature effects. This was particularly motivated by the previous observation that even small variations in structure, i.e., refractive index, could lead to large variation in the optical properties.

The temperature study started with a current transport simulation, performed by our collaborators in Politecnico di Torino, for reasonable working voltages (10 V applied voltage corresponding to more than 100 kA/cm^2). The results of their simulation are presented in Fig. 4.5. The calculated current densities were used to calculate the spatially varying internal Joule heating parameter, Q_J, defined as

$$Q_J = \frac{\overrightarrow{J_n^2}}{\sigma_n} + \frac{\overrightarrow{J_p^2}}{\sigma_p}, \tag{4.2}$$

where $\overrightarrow{J_n}$ and $\overrightarrow{J_p}$ are the electron and hole current densities and σ_n and σ_p are

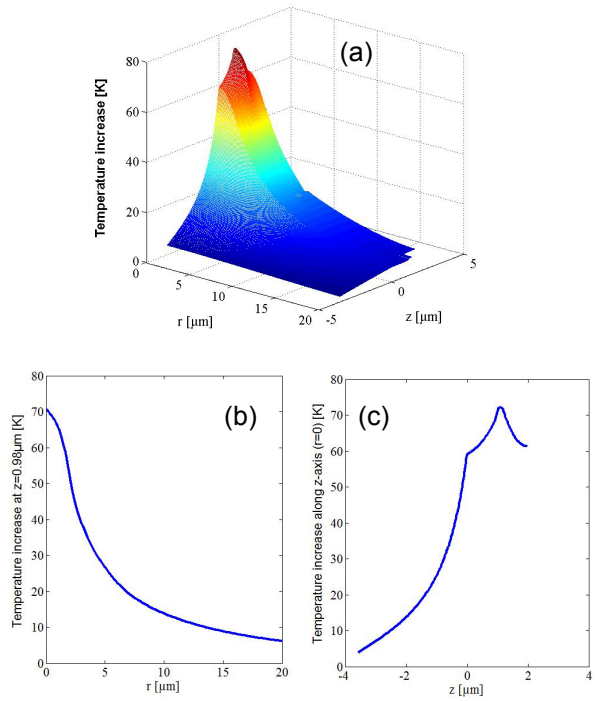

Figure 4.6: (a) Temperature distribution (from Joule heating) in the cavity, and (b,c) temperature profiles in two representative horizontal and vertical cross sections.

their respective conductivities. Solving the heat transfer equation with the calculated Joule heating as the source, the 2D temperature distribution was obtained, which is shown in Fig. 4.6.

The next step was to incorporate the temperature distribution curves into the 2D optical model and recalculate the effective refractive index changes in the presence of the temperature-induced change of the refractive index in the materials. For this, tabulated values for the thermo-optic coefficients of the cavity materials were used. The modified effective index distribution due to the self-heating is illustrated in Fig. 4.7.

The same temperature effects were also incorporated into the 3D optical model based on BPM, thus likewise modifying the refractive index distribution, after which the losses and the threshold material gains were calculated in the same manner as in the cold-cavity case. The final results are presented in paper C.

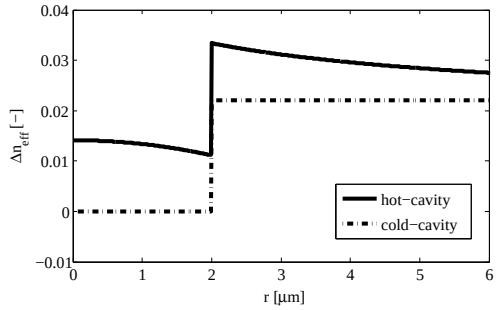

Figure 4.7: Change of effective refractive index n_{eff} due to temperature induced refractive index change.

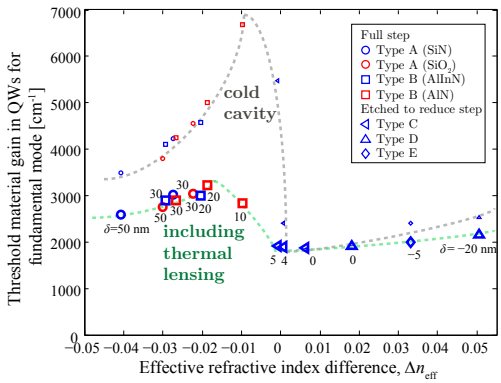

Figure 4.8: Calculated threshold gain for the fundamental mode in the different laser cavities. Small markers are for cold-cavities, whereas the corresponding larger markers indicate the results when thermal effects are included. The structural depression parameter δ is shown with negative numbers for elevated structures. Type A–E are the structural types of laser cavities shown in paper B and C.

4.3 The main conclusions

Figure 4.8 shows the threshold gain values for a large number of simulated cavities, both cold-cavity and with self-heating included, as functions of Δn_{eff}. Also indicated is the profile step δ of the cavity structure. It is evident from the figure that Δn_{eff} is a very good measure of the waveguiding ability of the cold cavity (Δn_{eff} is a property of the cold cavity for every structure), with $\Delta n_{eff}=0$ marking the border between antiguided, high threshold gain, and guided, low threshold gain, regimes. The figure together with other results from the simulations enable some important conclusions to be drawn.

- The guiding character of GaN-VCSELs can change strongly even for very small structural changes.
- The transition region close to $\Delta n_{eff}=0$ between the guiding and the anti-guiding cavities should be avoided due to the risk of having very high lateral losses.
- Cavities with fairly strong antiguiding have
  - Higher threshold gain than guided cavities, which further is temperature dependent and decreases with increased self-heating.
  - Built-in modal discrimination that is largely insensitive to self-heating.
- Cavities in guided regime have
  - The lowest threshold gain, which further does not depend at all on self-heating.
  - Lack of modal discrimination (in this case modal discrimination can possibly be obtained with e.g. shallow surface structures [113]).
- These findings have already had an impact, as several groups worldwide have implemented GaN cavities intentionally designed along these guidelines to enable lasing with reasonable threshold currents [62, 76, 78, 114, 115].

Chapter 5

Electrically conductive epitaxial III-nitride DBRs

5.1 GaN-based DBRs

Epitaxially grown DBRs can be advantageous for monolithic integration, and could possibly provide both high electrical and thermal conductivity. To achieve the high peak reflectivities (>99.5%) that are required for VCSELs, a high crystalline quality is important. This requires two epitaxial materials with small lattice mismatch, similar thermal expansion coefficients, and growth conditions that are suitable for both compounds, such as temperature [116]. Moreover, a high quality substrate with the right lattice parameter is also required. However, there is a lack of high quality low-cost substrates for III-nitride DBR growth, and foreign substrates are therefore used, which increases the complexity of the growth.

There is a tradeoff between the available refractive index contrast, lattice mismatch, and growth conditions to achieve high quality DBRs. As discussed in Chapter 3, two main III-nitride based DBR schemes have been implemented, $Al_xGa_{1-x}N$/ $Al_yGa_{1-y}N$ and $Al_xIn_{1-x}N$/GaN. The $Al_xIn_{1-x}N$/GaN system is lattice-matched for $x \simeq 0.18$, while the available refractive index contrast is 7.2% at 420 nm, and 6.4% at 450 nm. In the $Al_xGa_{1-x}N/Al_yGa_{1-y}N$ scheme, one can achieve a relatively higher refractive index contrast of 12 to 17% in the 420–450 nm wavelength range for the most extreme AlN/GaN case ($x = 1, y = 0$). However, for AlN/GaN DBR the lattice mismatch is as high as 2.5%, which easily can build-up in-plane tensile strain in the AlN layer and crack formation.

The $Al_xGa_{1-x}N$/ $Al_yGa_{1-y}N$ based DBR have been explored more extensively compared to AlInN/GaN DBRs. The growth window for AlInN is small and the growth rates to achieve high quality material has been low, when compared to AlGaN layers. However, in [117], it has been shown that by relatively high growth

temperature, and very low In/Al supply ratio the growth rate of AlInN layers can be increased up to $\sim$0.5μm per hour.

5.2 Mitigation of strain in AlN/GaN DBRs

As mentioned, the AlN/GaN DBR suffer from a 2.5% in-plane lattice mismatch where the high built in strain can easily result in crack formation. One option to mitigate the cracking is to use ternary AlGaN instead of binary AlN/GaN, but a larger number of pairs is then necessary to reach high enough reflectivity due to the lower index contrast, and the stopband width will thus be narrower. Different types of interlayers can be used at the interfaces to reduce strain in the DBR. For example, short-period superlattices (SLs) in AlN/GaN can be inserted either below the DBR structure [118], or incorporated inside the DBR [119]. Strain management can also be done by using low-temperature AlN interlayers [120]. The drawback of using strain compensating interlayers is their possible reduction of the overall DBR reflectivity, which has to be taken into account when designing the DBR [121].

Crack-free AlN/GaN DBRs without interlayers have also been shown by growth on SiC substrate, [122] and AlN substrates [123]. Selective-area-growth has also been applied to grow crack-free DBRs in areas up to 150×150 μm [124], sufficiently large for VCSELs.

5.3 Electrically conductive GaN-based DBRs

Most of the demonstrated electrically injected GaN-based VCSELs have so far suffered from lack of electrically conductive DBRs and therefore they have been imposed to use intracavity contacts with rather thick cavities to have reasonably efficient current injection into the device. The problems associated with long cavity designs are discussed in Chapter. 3. The main challenges to obtain electrically conductive III-nitride DBRs are the poor electrical conductivity of the individual layers, the large conduction band offsets, and the strong polarization fields along (0001) that limit the vertical current injection through these DBR.

There have only been a few reports on electrical conductivity in III-nitride-based DBRs. In 2002 Arita et al. [125], reported an n-type 26 pairs $Al_{0.4}Ga_{0.6}N$/GaN DBR with a series resistance of 180 Ω at high current densities. A 20 pairs $Al_{0.4}Ga_{0.6}N$/GaN DBR with RUGATE profile [126], showed a specific series resistance of 0.8 Ωcm^2 at high current densities. Ive et al. [127], demonstrated a highly reflective ($\geq$99%) crack free 20.5 pairs AlN/GaN DBR grown on SiC having a specific series resistances extracted from the IV-characteristics to be 0.1 Ωcm^2. Moreover, a differential specific series resistance of 2×10^{-4} Ωcm^2, has been reported, for a 40-pair $Al_{0.12}Ga_{0.88}N$/GaN DBR with a peak reflectivity of 92% at a wavelength of 380 nm [128]. The low Al-content AlGaN layers reduce the conduction band offset and thus contribute to high vertical conductivity, while the reflectivity is insufficient due to the low index contrast. Recently, Takeuchi and coworkers [69, 129], have obtained a specific series resistance of 1.7×10^{-4} Ωcm^2 using a 10-pair AlInN/GaN DBR with a specific modulation doping. They also incorporated a full 46-pair DBR

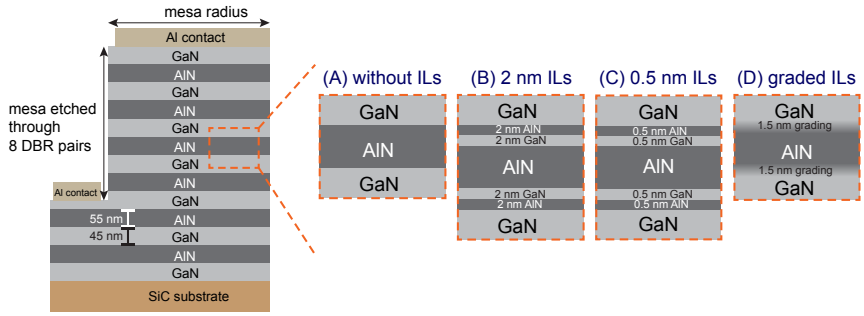

Figure 5.1: Si-doped AlN/GaN DBRs with different compositional interlayer schemes: (a) without interlayers (b) 2/2 nm AlN/GaN interlayers (c) 0.5/0.5 nm AlN/GaN interlayers, and (d) graded interlayers.

of the same type in a VCSEL, where the resistance of the full DBR was estimated to be 7.8×10^{-4} Ωcm^2.

5.4 Electrical characterization of the n-type AlN/GaN DBRs

At Chalmers University of Technology, research on epitaxial growth of undoped and doped AlN/GaN DBRs was pursued by PA-MBE. The structures were grown on SiC substrates, aiming to achieve a strain compensated state where the strain in the AlN and GaN layers are balanced. N-type doping using Si impurities with a dopant concentration of up to 2×10^{19} cm^{-3} was obtained.

In our study, four different DBR samples (A-D), each with 10.5 DBR-pairs, were grown with different interlayers at the heterointerfaces to explore their effect on the electrical conductivity of the DBRs, see Fig. 5.1. Sample A has no interlayers, samples B and C have one pair of AlN/GaN interlayers with thicknesses of 2 nm/2 nm and 0.5 nm/0.5 nm at each interface, respectively, and sample D has graded interlayers from GaN to AlN over 1.5 nm thickness, achieved by digital intermixing of Ga and Al sources. The transmission electron microscopy (TEM) images showed smooth layers with abrupt interfaces in the DBR structures, see Fig. 5.2. Optical microscope images of the surface for all samples are shown in Fig. 5.4. Cracks with micrometer lengths and sub-micrometer thicknesses covered all the samples and were present both prior and after processing. The corresponding atomic force microscopy (AFM) images of samples A–D for a scan size of 5μm$\times5\mu$m are shown in Fig. 5.5.

In order to measure the vertical resistivity of the 10.5 pair DBR samples, circular mesa structures with radii 45, 50, 75 and 100 μm were etched by RIE-ICP through 8 AlN/GaN pairs. Since the substrates used in this study had a limited bulk conductivity, it was not possible to form an ohmic contact neither on the top nor the bottom of the SiC substrate [130]. Therefore, mesas were dry etched on the samples

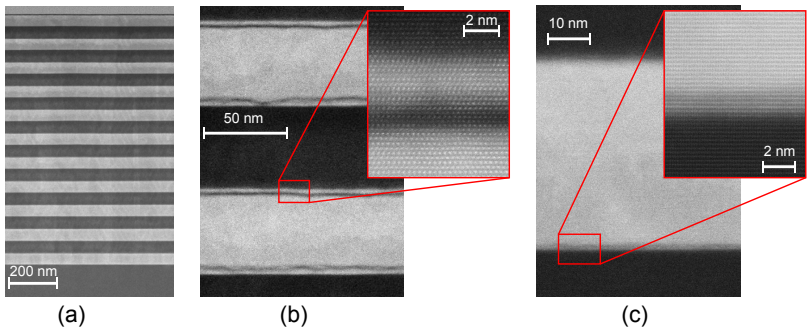

Figure 5.2: High-angle annular dark-field (HAADF) scanning transmission electron microscopy (STEM) images of (a) sample A, (b) sample B, and (c) sample C.

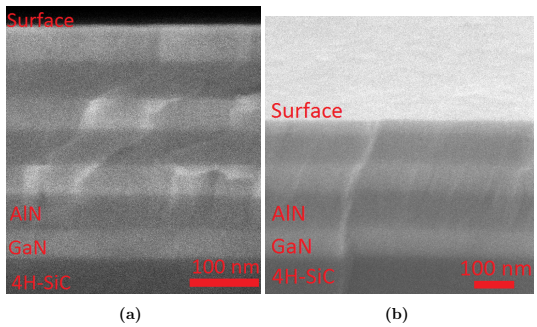

Figure 5.3: Cross-sectional SEM image of the remaining (a) 3.5 DBR pairs and (b) 2.5 DBR pairs, after dry etching of 7 or 8 pairs, respectively.

through 7 or 8 DBR pairs and the etch was stopped within an n-GaN layer. The SEM images showing the etch depths are shown in Fig. 5.3.

Next, ohmic contacts were to be deposited on top of the mesa as well as on the etched surface next to the mesa on the remaining 2.5 or 3.5 DBR-pairs. To obtain ohmic contact with low resistivity between metal and n-GaN, the contacts are usually annealed at high temperatures of approximately 700–900°C depending on the metal contact scheme and the doping concentration in the n-GaN layer. Such high annealing temperature can even exceed the growth temperature of the DBR layers. It was therefore much safer to find a metal contact scheme, for which thermal annealing could be avoided or at least only be done at more moderate temperatures below 600°C. Different metallization schemes were tested, where a 150 nm-thick Al contact yielded ohmic behavior with a specific contact resistivity of $\sim 10^{-4}$ Ωcm^2 without any annealing [131].

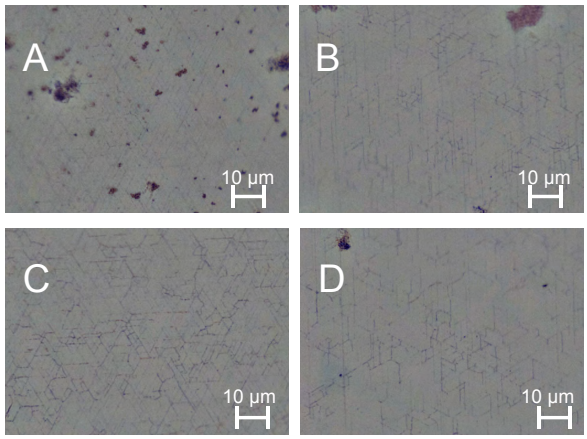

Figure 5.4: Optical microscopy pictures of Sample A-D. Cracks with micrometer lengths and sub-micrometer thicknesses are visible on all samples both before and after processing.

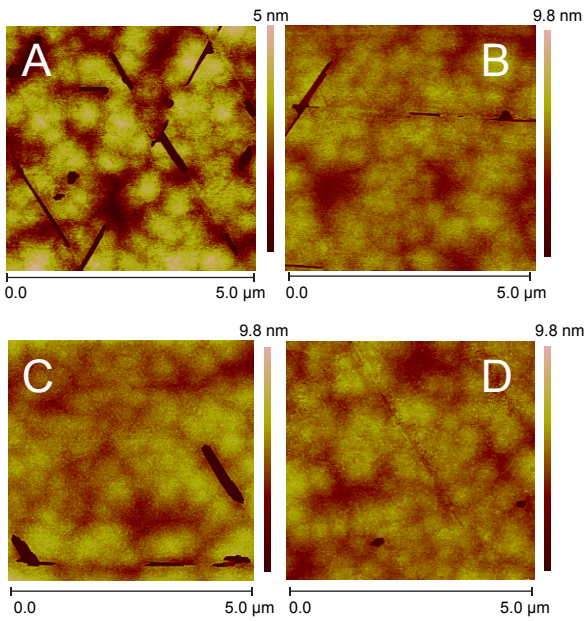

Figure 5.5: AFM images of samples A–D for a scan size of 5μm$\times 5\mu$m showing cracks with micrometer length and sub-micrometer thickness.

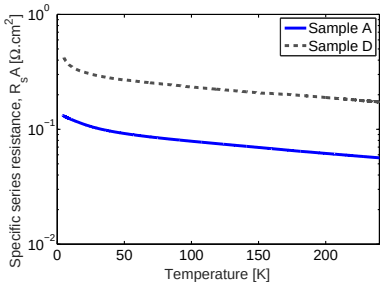

Figure 5.6: Low temperature dependence of the resistivity for a mesa structure with 100 μm radius for samples A and D.

5.5 The main findings of the study

I-V measurements were performed from RT down to 4 K, and specific series resistances were calculated for the four samples A–D. By comparing I-V characteristics of similar sized circular transmission-line method (TLM) patterns and mesas, the lateral and contact resistances are estimated to be <10% of the total measured series resistance. Sample A had a mean specific series resistance of 0.044 Ωcm^2 for 8 DBR pairs at low current densities. At higher current densities (of interest for VCSEL) the series resistance was reduced by ∼70%. Interestingly, sample A which had no interlayers showed lower resistivity compared to sample B–D with interlayers. This concludes that the incorporation of interlayers, necessary for strain compensation, can impair the vertical current transport through the DBR structure.

There was a concern regarding the contribution of the cracks and defects on the DBR samples to the overall conductivity. We have found multiple reasons to believe that in fact those cracks have not had any significant impact on the current paths:

- The mean specific series resistance for sample A (0.044 Ωcm^2 for 8 DBR pairs at low current densities) is comparable to the lowest values reported for similar n-type AlN/GaN DBRs that were crack-free [127].
- In the low temperature I-V characteristics down to 4 K, the resistivity increased only by a factor of 3, see Fig. 5.6, which is also very similar to that of the previously reported n-type AlN/GaN DBRs [127].
- The mean specific series resistance, R_sA do not change with mesa size. This proves that the current injection through the DBR structures have been uniform across the entire mesa area.

Thus we believe that the cracks are not the major contributor to the vertical electrical conductivity in our DBRs. Even though the DBRs with no interlayers showed state-of-the-art conductivity for AlN/GaN DBRs, a lot more can be explored to increase the conductivity such as compositional gradients, modulation doping, and utilizing the polarization fields.

Chapter 6

High contrast grating reflectors for GaN VCSELs

The behavior of optical gratings has been known for a long time since their discovery in the 16th century and they have been used to a wide extent in monochromators, spectrometers, and optical filters. The principle behind these periodically varying structures is based on diffraction, the splitting of a light beam into several diffracted beams propagating in different directions. Thus they are often referred to as diffraction gratings. By definition, in the diffraction regime the grating period, Λ, is larger than the wavelength of light, λ. The recent progress in micro/nano fabrication has made it possible to shrink the dimensions of gratings, where the period can become close to the light wavelength. It was found that structures in this so-called near sub-wavelength regime ($\Lambda \leq \lambda$) has different optical features and therefore the gratings has become a very interesting topic again in the 21st century for new applications. Moreover, in the extreme case of the deep sub-wavelength region ($\Lambda \ll \lambda$) the grating dimensions are too small and they appear as a homogeneous medium to the incident light.

In 2004, Hasnain and coworkers proposed that if a one-dimensional (1D) near sub-wavelength grating structure with high-index grating bars is fully surrounded by low-index media (such as air), the grating structure can have extraordinary optical features such as high reflectivity $> 99\%$ over a broad bandwidth, $\Delta\lambda$ ($\Delta\lambda/\lambda > 30\%$), and high quality factor resonance, $Q > 10^7$. These gratings were called high contrast gratings (HCGs) since the high index contrast was claimed to be the essential factor for these significant properties. Since then the HCG field has rapidly expanded with both experimental demonstrations and theoretical explanations for the spectacular reflectance properties of HCGs.

The high reflectivity over a broad bandwidth have made HCG structures great candidates to substitute the DBRs in VCSELs. The HCGs in fact can provide a couple of extra advantages compared to the already well-established DBRs, such as

polarization selectivity, wavelength setting capability for multiple-wavelength VCSEL array, transverse mode control for single-mode devices, improved tuning speed and range for tunable VCSELs, among others. Another feature related to VCSELs is the possibility for beam steering and focusing [132, 133].

Beside replacing DBRs, HCGs can have some other interesting applications due the ultra-high Q-factor resonances such as HCG-based resonance cavities with surface normal emission for displays, sensing, and communication applications [134].

6.1 Structural description

The schematic of a part of HCG structure is illustrated in Fig. 6.1, assuming an infinite number of grating beams which are infinitely long, or at least that the grating extends far beyond the area illuminated by the incident light beam. The grating structure has a thickness of t_g, width of ω, and period of Λ. The duty cycle or the fill factor is defined as the ratio between the grating beam width and the period (ω/Λ). The grating material is normally chosen to have a high refractive index of n_g, which is surrounded by a low index material n_l, preferably air, which has the lowest index. In the case of having an air-suspended HCG, i.e., grating beams entirely surrounded by air, the parameter a_h is referred to as the airgap. The two polarizations of a normally incident plane wave, transverse-electric (TE) and transverse-magnetic (TM), are defined as having the electric field parallel to the grating beams and perpendicular to the grating beams, respectively, as shown in the figure.

The fundamental working mechanism of HCGs have been explained and analytical formalisms have been published, which are reviewed thoroughly in [135]. Two main physical pictures have often been introduced: one based on guided-mode resonance (GMR), also called leaky modes, and the other based on waveguide array mode, also known as Bloch mode theory. A simplified intuitive picture using the latter approach can be obtained where the grating is seen as a periodic array of short slab waveguides, supporting two waveguide array modes. As explained before, when Λ shrinks to values near λ only the 0-th diffraction order can carry significant energy, either in reflection or transmission. This is called the dual mode regime where only two waveguide array modes are propagating inside the grating and the 0-th order diffracted beam is propagating outside the grating. If the parameters of the grating are designed properly, e.g. the grating thickness is set such the accumulated phases of the waves passing through the grating beams and the air spacing in between them allow for a destructive interference at the output plane, the optical power will be launched back to the low index medium and thus reflectivity will, in theory, be equal to unity.

6.2 HCGs as broadband reflectors for VCSELs

Up to now, only a few electrically-pumped HCG-VCSELs have been realized, and mainly in infrared wavelength regime. There are a few examples where the HCG is incorporated as part of the top reflector in combination with a few DBR pairs, for emission wavelengths at 850 nm [136], 980 nm [137], and 1550 nm [138], using

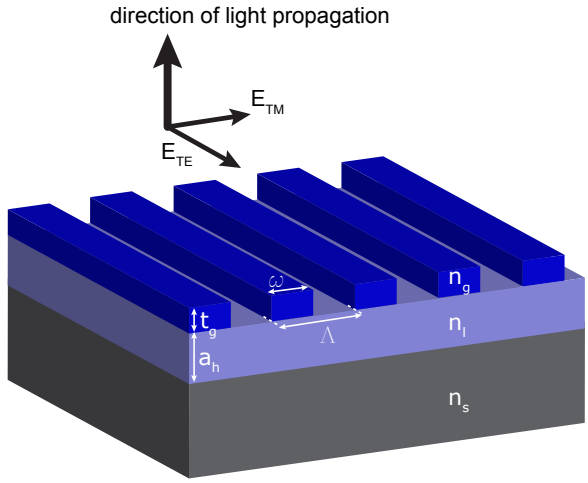

Figure 6.1: Schematic of HCG with a high index grating material (n_g), low index material (n_l), and substrate index (n_s). HCG parameters are the layer thicknesses t_g and a_h, period Λ and duty cycle ω/Λ.

AlGaAs/air, GaAs/oxide, and InP/air HCGs, respectively. However it was shown in two other experiments that the top DBR can be completely substituted by a HCG with high enough reflectivity, in devices employing GaAs/air HCG at 980 nm [139] and 1060 nm [140], and Si/SiO_2 HCG at 1320 nm [141] wavelength. Worth to mention is also an optically pumped VCSEL using two HCGs as the top and the bottom reflectors, which proves the concept of DBR-free VCSELs [142].

Thus there are hopes that HCGs can be a solution for one of the key challenges in GaN-based VCSELs at UV-blue-green emission wavelengths, the realization of high quality feedback mirrors. This is very demanding in GaN-based DBRs due to relative small index-contrast and/or the large lattice mismatch in this material system. In addition to the high reflectivity and wide reflectivity stopband, HCGs can offer post-epitaxial wavelength setting [139], which can be desirable for GaN-VCSELs suffering from growth inhomogeneities.

Some groups have consequently attempted to realize III-nitride membrane type HCG structures for the visible regime, in spite of difficulties in this material system to obtain wet etch selectivity and thereby achieve an airgap below the grating in a simple way. For instance, bandgap-selective PEC etching of InGaN superlattice layers has been performed to make AlGaN gratings, but with limited airgap height [143], and a focused-ion-beam (FIB) etching process was employed to drill a large airgap underneath a GaN grating pattern [144]. In addition, GaN HCGs using GaN-on-Si have been demonstrated by backside Si wafer etching [145, 146]. However the integration to VCSELs will be very difficult since high enough quality growth of epi-on-Si is still extremely challenging. Due to this technological problem, Lee

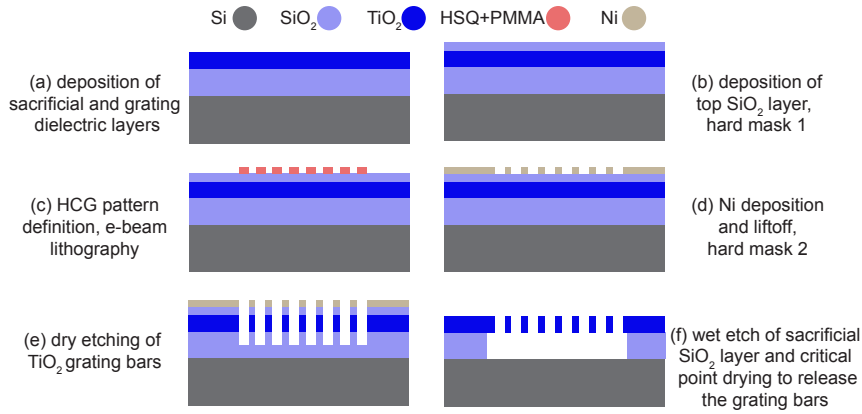

Figure 6.2: Schematic of HCG fabrication steps.

et al. [147], have proposed a GaN grating reflector with no airgap. Although this scheme is more mechanically rigid, the fabrication tolerance for reflectivities higher than 99% will be much smaller, suggesting that the air-suspended type should be preferred. Another example with no air-suspension is an optically pumped GaN-based VCSEL using a photonic crystal HCG [148], in which the grating pattern is drilled down to about 0.5 μm through the multiple quantum wells.

In this chapter, the details about design and fabrication of a free-standing dielectric HCG suitable for the visible regime, made of TiO_2 material, are discussed. Among the dielectrics, TiO_2 has a high refractive index of about 2.6, similar to that of GaN, with a negligible absorption for wavelengths longer than 400 nm. As a dielectric sacrificial-etch layer SiO_2 is suitable, providing an extremely high wet etch selectivity. This scheme leads to a robust way of direct integration to different material systems since the lattice matching is not a prerequisite and the residual stress in the dielectric films can be tailor-made to a value that, in the end, yields grating beams that do not buckle or bend.

6.3 Fabrication of TiO_2/air HCG

The fabrication steps of the TiO_2/air HCG are summarized schematically in Fig. 6.2. In our case, the as-deposited TiO_2 film using the standard deposition parameters resulted in very good optical (high refractive index and low absorption) and chemical (high wet-etch selectivity) properties, but the mechanical residual stress had to be modified. This modification in the deposition parameters led to different dry etching behavior by the film, so thereby the process parameters of the dry etching had to be optimized as well. Moreover, both the residual stress and the dry etching behavior significantly depended on an optional annealing process. This interplay and mutual dependence between the processes were the main challenges of this work.

Dielectric stack deposition

The first step in the fabrication is the deposition of the dielectric stack. As seen in Fig. 6.2, in addition to the SiO_2 sacrificial layer and the TiO_2 grating, an extra SiO_2 layer is used to improve the dry etch profile of the TiO_2 gratings. The fabrication details of the dielectric stack are summarized in Table 6.1. The SiO_2 was deposited by PECVD since it yielded a less dense film, suitable for removal by wet etching. Sputtering was the only available method for TiO_2 deposition, where the RF bias power could be varied to modify the residual stress of the film.

Table 6.1: Fabrication details of the dielectric stack.

No.	Process step	Tool	Process parameters
1	bowing (stress) measurement of 2-inch Si substrate	Tencor surface profilometer	-
2	SiO_2 deposition	PECVD-Oxford plasmalab 100 system	standard recipe
3	bowing (stress) measurement after deposition	Tencor surface profilometer	-
4	TiO_2 deposition	Sputtering-FHR MS150	1 kW dc power, $5{\cdot}10^{-3}$ mbar, 40 sccm Ar flow, 4 sccm O2 flow, 300–400 W RF bias power
5	bowing (stress) measurement after deposition	Tencor surface profilometer	-
6	SiO_2 deposition	Sputtering-FHR MS150	1 kW RF power, $1.2{\cdot}10^{-2}$ mbar, 40 sccm Ar flow, 15 sccm O2 flow

Controlling the residual stress

The residual stress measurement done by simple wafer bow technique revealed >+300 MPa tensile stress in the initial TiO_2 film. However the incorporated stress in the final fabricated gratings could change during the subsequent process steps, and a more sophisticated technique will be required to determine the stress locally near each structure [149]. Nevertheless, in the first attempt to cope with the high residual stress in the TiO_2 film, a stress-relieving trench around the grating was deployed, which in some cases helped to reduce the bending of the grating beams, but unfortunately led to tilting or sagging of the whole structure, see Figs. 6.3c and 6.3d. Therefore, the deposition conditions of the TiO_2 film were instead optimized, to reduce the tensile residual stress. Among the tested parameters, the dc power, the RF bias, and the temperature (during deposition)- no dependence of the film stress on the dc power was observed.

Thermal annealing can strongly affect stress in the TiO_2 film and make it more tensile. Thus to produce a low stress film it was important to minimize the self-

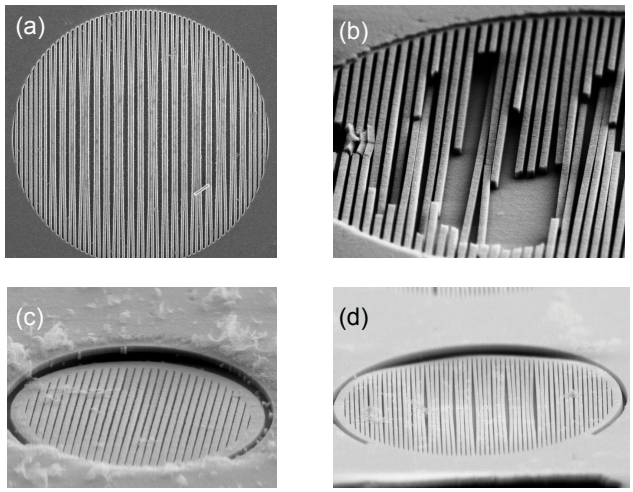

Figure 6.3: SEM images of released TiO_2 gratings with too large stress in the film (+300 MPa). (a,b) Severe bending of TiO_2 grating beams which can even lead to breaking. (c,d) Released TiO_2 gratings with stress-relieving trenches which reduced the bending to some extent, but instead caused tilting and sagging of the whole structure.

heating that can occur during the TiO_2 sputtering, in which the substrate temperature could rise up to 300°C in a 30 minutes deposition which was required to achieve the desired TiO_2 thickness. Several deposition interruptions were used (5 minutes deposition/ 5 minutes cool down in load lock and open air in total) to minimize the heating. In addition, the wafer was mounted with thermal tape on a copper chuck to improve the heat dissipation, as illustrated in Fig. 6.4a. The mounting could also result in a more uniform temperature distribution across the wafer and an thereby improved stress uniformity.

Beside the self heating, an RF bias power supplied to the substrate holder could strongly affect the stress in the film, where a higher RF bias power resulted in more compressively stressed films. A number of tests were carried out with different RF bias values, and the resulting stress in the TiO_2 film, measured by wafer bowing technique is shown in Fig. 6.4b. The optimum RF bias was around 300 W, which resulted in a slightly compressive stress in the film. No bending or buckling could be observed in the released gratings whose TiO_2 films had an initial compressive stress ranging from 0 to -100 MPa.

Pattern definition and Ni lift-off

The HCGs were defined on the sample using electron beam (e-beam) lithography. A bilayer of hydrogen silesquioxan (HSQ) and poly-methyl-methacrylate (PMMA-A2)

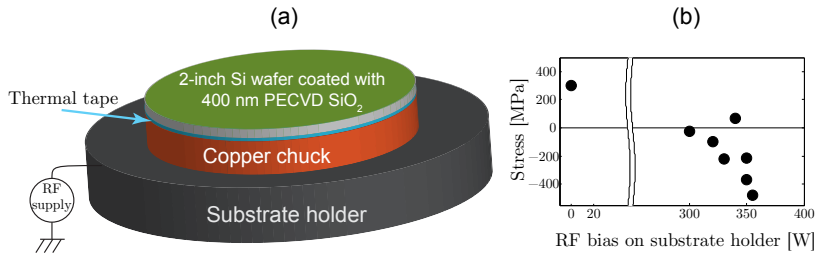

Figure 6.4: (a)Schematic of the mounting of the wafers on the copper heat sink to improve the heat dissipation and minimize self-heating during TiO_2 deposition. (b) Stress in the TiO_2 film as a function of different RF power supplied to the substrate.

was utilized as it has proven well-suited for sub-10 nm resolution of the Ni pattern after lift-off [150]. A 50 nm thick Ni layer was evaporated onto the developed resist using an e-beam evaporation system followed by lift-off to create the required hard mask for the etching process.

Dry etching

The full description of the dry etching is in Paper E. In brief, the metal-oxides are etched with fluorine based gases, among which CHF3 has the advantage of forming controlled amount of fluoro-carbon polymers that can help protecting the side walls. With the right amount of CHF_3 and the right value of the plasma power good directionality can be obtained. By having a low pressure (<5 mTorr) and certain amount of electrode RF power (75 W) and ICP power (125 W) a good control of the etch rate and vertical sidewalls of TiO_2 grating can be obtained, even when the dielectric film is not annealed.

After etching the cross-sections of the gratings were characterized using Scanning Electron Microscopy (SEM) to measure the duty cycle of the grating, to check the slope of the sidewalls of the grating, and to ensure that the etch had continued deep into the sacrificial SiO_2 layer. With a too shallow etch into the bottom SiO_2 layer the wet etch of the sacrificial layer would be more difficult and time consuming.

Sacrificial layer removal by wet etching

The Ni hard mask was first removed in a °C-Cr/Ni wet etch solution for 15 minutes Next, the sacrificial SiO_2 layer was removed in a diluted mixture of Buffered-Oxide-Etch (BOE) and water with a 1:5 ratio for 4 minutes to selectively etch away the SiO_2 and release the grating structures. Finally the sample underwent a critical point drying, to prevent the grating bars from bonding to the substrate by capillary forces.

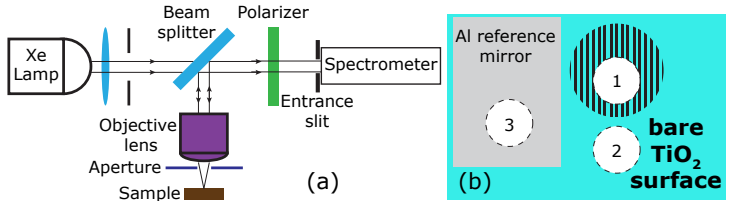

Figure 6.5: (a) Schematic of the micro-reflectance setup. (b) For calculating the absolute reflectance three reflectance spectra were captured in the regions on the sample indicated by circles, the sizes of which roughly indicate the diameter of the incident light beam; region 1 on the grating; region 2 on the adjacent bare TiO_2 surface; and region 3 on the Al reference mirror.

6.4 Characterization of TiO_2/air HCG

The fabricated HCGs have a small diameter, usually $<20\mu$m, and they are designed for normal incident reflection since they are intended for placement on top of the VCSEL mesa. This makes it challenging to measure the reflectivity spectrum of the HCGs. In such characterization the incoming light must have a spot size less than the diameter of the HCG, and impinge on the grating surface with a normal angle. Therefore, lenses are used to focus the incoming light down to the desired size. However, in this case, the numerical aperture of the lens determines the range of the angles within which the incoming light hits the grating surface. Therefore, a narrow pinhole has to be used to limit the acceptance angle as much as possible.

As is illustrated in schematic in Fig. 6.5a, a micro-reflectance measurement setup was used to evaluate the optical performance of the realized HCGs. In this setup, incoming light from a Xe white light source is tightly focused with a lens, a circular pinhole and a microscope objective (100×, numerical aperture=0.5) to a spot size of about 5–10 μm on the grating. This is sufficiently small since the characterized gratings had a diameter of 12 μm. A second pinhole (1.5 mm opening) is placed beneath the objective at a distance of 7 mm from the sample surface to limit the acceptance angle of the incident and collected light. The acceptance angle in horizontal direction is defined by this aperture ($-6^\circ < \theta_\perp < +6^\circ$), while the acceptance angle in vertical direction is defined by the 300 μm narrow entrance slit of the spectrometer ($\theta_\parallel < \theta_\perp$). Moreover, a polarizer is inserted in the light path to allow for measuring the reflectivity of TE and TM polarized light, i.e., characterize the polarization dependent reflectivity spectrum.

In order to define the absolute reflectance value (or the 0-th order reflected diffraction efficiency, to be precise) from the HCG, a reflectivity spectrum is recorded not only from the HCG, but also from an Al-reference mirror and from the TiO_2/SiO_2 stack nearby the HCG, as indicated in Fig. 6.5b. The spectrum acquired from the HCG is divided by the reflectivity spectrum of the Al reference mirror. However, the obtained value will be overestimated due to the fact that Al has a reflectivity of only ~90% in the visible spectrum. Therefore, by measuring the reflectivity of the

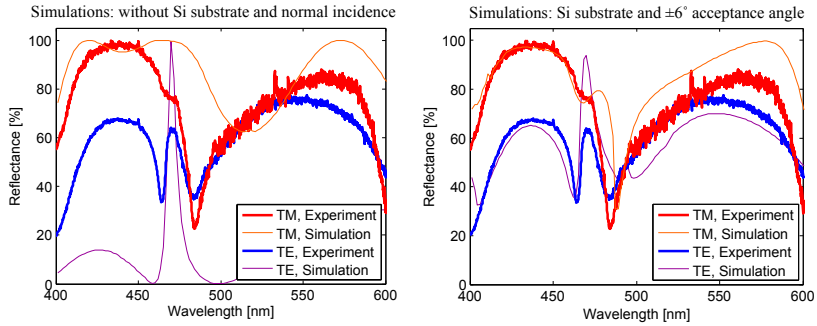

Figure 6.6: Measured reflectance spectra of the TiO_2 HCG with a period of 370 nm, a duty cycle of about 45%, a grating layer thickness of 210 nm and an airgap of 340 nm, for both TM and TE polarized light, and (a) simulations assuming only normally incident light and no Si substrate and (b) simulations accounting for a finite acceptance angle of 6° and the underlying Si substrate.

TiO_2/SiO_2 stack adjacent to the grating (region 2 in Fig. 6.5b) and comparing it with its numerically simulated reflectivity spectrum, an almost wavelength independent normalization factor of 1.2 is easily estimated that accounts for the imperfect Al-reference. The measured spectrum from the grating is then divided not only by the Al reference mirror reflectance but also by the normalization factor to realistically calculate the absolute values for the reflectance spectrum.

Figure 6.6 contains the extracted reflectance spectra for both TM and TE polarized light. Peak reflectance values exceeding 95% near the center wavelength of 435 nm with a FWHM for the stopband of about 80 nm are achieved for the TM polarized light. The peak reflectance for the TE polarized light is however only 30% lower which is a much smaller difference than the theoretical predictions indicate. This is because it is not possible to isolate the reflectivity of the HCG from that of the structure beneath. The HCG is poorly reflective for TE polarized light and therefore a large reflection comes from the air/Si substrate interface. To get a good agreement between measured reflectivity spectrum and simulated it is important to also consider the finite acceptance angle of 6° in the measurement set-up, which is included in the simulations by averaging the reflectance values for different angles of the incoming light. The difference between including and not including non-normally incident light and the underlying Si substrate in the simulations can be seen by comparing Figs. 6.6a and 6.6b. A very good match between the the rigorous coupled-wave analysis (RCWA) simulations and the measurements can be obtained when the Si substrate and the acceptance angle is accounted for in the model. In this simulation the refractive index dispersion of TiO_2 is incorporated from the measured ellipsometry data.

Chapter 7

Outlook and future directions

The future for the GaN-based VCSELs is very bright thanks to the many possible applications, both expected and unforeseen ones. To get an idea about how long time it will take until the GaN VCSEL is commercially available and produced in large volumes, one can take a glimpse at the history of the GaAs-based VCSEL. The GaAs-based VCSELs were outlined briefly in the introduction chapter, starting with the first demonstrations by Iga in 1977. However, it was not until 18 years later that Honeywell (later acquired by Finisar Co.) commercialized them, showing the time and the effort it usually takes from a demo to a reliable high-performance device. The fact that three large companies (Nichia, Panasonic, and Sony) have put so much effort in violet-blue-green GaN-based VCSELs indicates that they believe that there is a big commercial value in this field. In addition, the increased number of research groups that have demonstrated lasing action during recent years, and the increased number of contributions at conferences show the interest this field has arisen. It is expected that many more applications for UV-blue-green VCSELs will appear once such light sources are commercially available.

The prospects of the GaN-based VCSELs and the future directions depend on understanding the challenges and shortcomings of the current technologies. Based on the challenges that were explicitly introduced in Chapter 3, here follows an outlook and suggestions for future work for the electrically pumped GaN-based VCSELs.

Developing an efficient scheme to laterally confine the current with low electrical and optical loss is essential to achieve high-performing devices. In long wavelength InP-based VCSELs, buried tunnel junction (BTJ) structures have proved to be a smart way to confine the current to the center of the device [105]. In addition, it enables the resistive p-type layer to be replaced by highly-conductive n-type material. This would also be a great benefit in the GaN-VCSEL, since it would provide efficient lateral current spreading without the use of ITO. The ITO has a high optical absorption and poor electrical contact to p-GaN, as described in Section 3.2.4, and

is a major contributor to the poor performance of GaN-VCSELs. In addition, a TJ would remove the need for contacts to p-GaN, since there will be n-GaN on top of the device instead, allowing for low-resistive ohmic contacts to be formed. Tunnel junctions in III-nitride materials is a challenge to achieve due to the wide bandgaps of the materials combined with low doping concentrations, in particular p-type doping. However, in recent years a lot of progress have been done in the field, where low-resistance tunnel junctions have been demonstrated using strained InGaN [151–153], Gd-nano islands [154, 155], and highly doped GaN [156, 157]. The GaN TJs are perhaps the most promising considering that also the optical losses have to be kept low. The Ohio group has showed a highly doped GaN TJ with a very differential resistance of $10^{-}5\ \Omega\text{cm}^2$ and ability to withstand high current densities of 150 kA/cm^2 [158]. GaN TJs have also been implemented in LEDs by the EPFL team where they have demonstrated a differential resistance of the TJ of $10^{-}4\ \Omega\text{cm}^2$, and ability to withstand high current densities exceeding 20 kA/cm^2, necessary for the implementation in VCSELs. There has so far only been one demonstration of a TJ GaN VCSEL by the USCB team [77], but there will most likely be more in the near future. A BTJ may be a good scheme for lateral current confinement, but it may race concerns about how it affects the optical properties of the device, such as optical absorption and optical guiding. We have seen that an elevation in the center of the structures, as the one created by a BTJ, can modify the optical guiding properties of the VCSEL [112] and would thus be very important to consider.

The work on electrically conductive III-nitride-based DBRs is still of interest to pursue even though the recent low resistivity n-type AlInN/GaN DBRs by Meijo University has almost reached the level to be practically used in GaN VCSELs [69]. The remaining challenge in the conductive AlInN/GaN DBR is the narrow reflectivity stopband and the high number of DBRs needed (>46 pairs). Any deviation in thickness of the DBR layers will translate into a deviation in the center position of the stopband, for example a 3% thickness deviation, results in a 3% shift of the center position of the DBR stop-band, which corresponds to 12.5 nm if the mirror is designed for 420 nm. A broader stopband DBR makes the spectral alignment between DBR reflectivities more easy as well as their matching with gain spectrum and cavity resonance. The newly demonstrated ZnO/GaN DBRs [159] seem to be promising as the research is still ongoing on combining the epitaxy of those materials. ZnO and GaN are nearly lattice matched and the available refractive index contrast can provide sufficient reflectivity with 20 DBR pairs and a wider stopband. The low conduction band offset and high doping levels that can be obtained are promising for the vertical conduction in such DBRs. Another interesting path for conductive III-nitride DBRs, is the combination of normal GaN layers and nano-porous GaN, obtained using conductivity based electrochemical etching (ECE). The ECE has been used to make GaN/airgap DBRs [160] as well as GaN/porous-GaN DBRs [161], were in the former the available index contrast is maximized and in the latter sufficiently index contrast (controlled by the porous size) can be obtained. The GaN/porous-GaN DBRs are promising as they can be expected to provide larger thermal conductivity and more mechanically stable structures as compared to GaN/airgap DBRs, in addition to simple growth due to absence of lattice strain. Furthermore, the incorporation of doped n-GaN layers should also lead to electrical conductivity in the

GaN/porous-GaN DBRs [162].

The double dielectric VCSEL scheme is also of interest to pursue, since dielectric DBRs provides high peak reflectivities and broad stopbands. Substrate lift-off technique have been presented in Chapter 3, where the following approaches are very interesting; the bandgap-selective PEC method [67], high wet etch selectivity between GaN and AlInN [163] and GaN and ZnO [164]. In addition, the conductivity-selective electrochemical etching of n-GaN layers can also be useful for substrate lift-off [165].

An alternative to DBRs is high contrast gratings, where in addition to high peak reflectivities and wide stopbands also polarization selection, transverse mode control and wavelength setting by the grating parameters can be achieved, as outlined in Chapter 6. The ZnO/GaN hetero-epitaxy [166] can be interesting to fabricate novel free-standing GaN-based HCG structures for GaN VCSELs, owing to the high wet etch selectivity between ZnO and GaN. Another approach is to use monolithic high contrast grating (MHCG), which recently were proposed [167]. It is shown theoretically that a very high reflectivity >99.9% can be obtained even without any airgap in the HCG structure. The MHCGs, as opposed to ordinary HCGs, are more mechanically rigid and better for current injection. However, due to the lack of high index contrast in the vertical direction, the fabrication tolerance window for these type of structures is expected to be more narrow

Finally, electrically pumped GaN-based VCSELs in the violet-blue spectral range have reached reasonably good performances in terms of milliwatt-class optical output power ($\sim$3 mW) at moderate injection current densities ($\sim$10 kA/cm^2). There is however still work that needs to be done when it comes to the electrical injection in the devices. GaN-VCSELs usually degrade after just a few minutes of operation, due to the poor electrical contact between the p-GaN and the ITO. This is an issue that must be solved before GaN VCSELs can be of real use in applications. Spurred by the progress in violet-blue-emitting VCSELs, the trend is now to push to shorter wavelength in the UV range [168, 169]. The realization of electrically injected AlGaN-VCSELs is very challenging due the difficulties in terms of p-type doping and material quality, for instance in DBRs, but can open up a new range of applications in the UV regime such as in bio/chemical photonics, water purification, medical devices, and material processing [170].

Chapter 8

Summary of Papers

Paper A

"Engineering the Lateral Optical Guiding in Gallium Nitride-Based Vertical-Cavity Surface-Emitting Laser Cavities to Reach the Lowest Threshold Gain", *Japanese Journal of Applied Physics*, , vol. 52, no. 8S, p. 08JG04, May 2013.

By using numerical simulations (2D effective index method and a 3D coupled-cavity beam propagation method), it is shown that the standard approach used by most groups to confine the current to the center of the VCSEL by using a dielectric aperture, will result in optically antiguided structures with high optical losses and thus very high threshold gains. To avoid the detrimental effect of lateral leakage and high diffraction loss, new structures are proposed where an elevation near the optical axis is achieved by additional processing. The proposed structures are estimated to reduce the threshold material gain by a factor of three, from 6000 to 2000 cm^{-1}.

My contribution: I, together with Åsa Haglund, came up with the original idea that minor structural changes in the realization of current apertures may have a massive effect on optical loss. I developed an intuitive physical model that explained this phenomenon as a transition between a guiding and antiguiding cavity. This motivated and guided the in-depth numerical work described in Papers A-C. More specifically, in Paper A, I proposed suitable cavity structures to be studied and performed the simulations based on 2D effective index method and analyzed the 2D and 3D simulation results. I wrote the manuscript, with feedback from the co-authors.

Paper B

"Analysis of structurally sensitive loss in GaN-based VCSEL cavities and its effect on modal discrimination",*Optics Express*, vol. 22, no. 1, pp. 411–426, Jan. 2014.

Motivated by the optical guiding and anti-guiding phenomenon studied in Paper A, a set of cavity structures with different guiding properties are explored in more detail by estimating the contributions of outcoupling (mirror) loss, material absorption, and lateral loss to the total optical loss. It is shown that the lateral loss is extremely sensitive to nanometer-sized changes in the cavity structure. Moreover, the remarkable reduction of the threshold gain with increased anti-guiding effect is analyzed. It is shown that for strong enough anti-guiding, the resonant lateral leakage loss decreases which leads to more tolerable threshold gain values. This anti-guided regime was previously suggested for robust single-mode operation due to a very strong suppression of higher order modes. Using simple analytical formulas, based on analogies with slab waveguides, a factor of $\sim$4 increase in modal discrimination was expected. However, our simulations indicate that for the VCSEL cavities the increased lateral losses for the first higher order mode is typically 50–100%, thereby the modal discrimination is high but less significant than expected.

My contribution: I proposed the set of different cavity structures to be studied and performed the simulations based on 2D effective index method. I contributed to the analysis and wrote the paper together with Jörgen Bengtsson, with feedback from the co-authors.

Paper C

"Thermal lensing effects on lateral leakage in GaN-based vertical-cavity surface-emitting laser cavities", Submitted to *Optics Express*, Nov. 2016.

This paper is an extension of paper A and B by including thermal lensing effects on the guiding and anti-guiding properties. Threshold material gain, optical loss, and modal discrimination are recalculated to realistically account for the substantial Joule heating in the GaN VCSEL cavities. The induced thermal lensing does surprisingly not make antiguided cavities more positively guided, so that they would approach the unguided regime with extremely high lateral leakage. Instead, thermal lensing strongly suppresses the lateral leakage for both anti-guided and guided cavities. This is explained in terms of lowered launch of power from the central part of the cavity and/or lower total internal reflection in the peripheral part; the former effect is active in all cavities whereas the latter only contributes to the very strongly reduced leakage in weakly antiguided cavities. Thermal lensing suppresses lateral leakage both for the fundamental and the first higher order mode, but a strong modal discrimination is still achieved for the antiguided cavities. Thus, strongly antiguided cavities could be used to achieve single-mode devices, but at the cost of slightly higher threshold gain and stronger temperature dependent performance characteristics.

My contribution: I proposed the different cavity structures to be studied and performed the simulations based on 2D effective index method. I provided input in terms of device structure and operating conditions for the electrical current transport calculations and contributed with data on thermo-optic coefficients for the temperature dependent refractive index profile calculations. I participated in the analysis and wrote the paper together with Jörgen Bengtsson, with feedback from the co-authors.

Paper D

"Effect of compositional interlayers on the vertical electrical conductivity of Si-doped AlN/GaN distributed-Bragg reflectors grown on SiC", Submitted to *APL Photonics*, Nov. 2016.

A highly reflective and electrically conductive DBR is one of the major challenges in GaN-VCSELs. In this paper the electrical characteristics of Si-doped AlN/GaN DBRs grown by plasma-assisted molecular beam epitaxy on SiC substrates are experimentally investigated with a focus on the effect from strain-compensating interlayers on the vertical conductivity. The DBRs without interlayers yield a state-of-the-art specific resistance of 0.044 Ωcm^2, while DBRs with interlayers show higher resistances between 0.16 to 0.34 Ωcm^2.

My contribution: I, together with Filip Hjort, developed a contact technology for non-alloyed contacts to n-GaN and processed mesa structures from the epitaxially grown n-doped AlN/GaN DBRs to perform vertical I-V measurements through the DBRs. I contributed to the DBR characterizations, data analysis, and wrote the paper with feedback from the co-authors.

Paper E

"TiO_2 membrane high-contrast grating reflectors for GaN-based vertical-cavity light emitters", *Journal of Vacuum Science & Technology B*, vol. 33, no. 5, p. 050603, Sept. 2015.

To circumvent the difficulties in creating free-standing HCGs in III-nitride-based materials due to their resistance to wet-chemical etching, it was here proposed to instead use dielectric materials. TiO_2 was used as the grating material since it offers a similar refractive index contrast as free-standing gratings in GaN and yields a high wet etch selectivity to the sacrificial layer of SiO_2 used below. The developed fabrication process yields grating bars with low built-in stress and thus no bending, and with a near-ideal rectangular cross sectional profile. This is the first demonstration of TiO_2-based HCGs and the measured optical reflectivity spectra of the fabricated high contrast gratings show very good agreement with simulations, with a high reflectivity of >95% over a 25 nm wavelength span centered around 435 nm for the transverse-magnetic polarized light.

My contribution: I did the vast majority of the work for this paper. I designed the HCGs based on rigorous coupled wave analysis. I developed the fabrication process involving deposition of low stress TiO_2, e-beam lithography using bilayer resist to define the grating bars, and dry etching optimization to create vertical sidewalls. I measured the reflectivity spectra of the HCGs using a micro-reflectance setup and compared them to my simulated spectra. I wrote the paper with feedback from the co-authors.

References

[1] Å. Haglund, J. S. Gustavsson, J. Vukusic, P. Modh, and A. Larsson, "Single fundamental-mode output power exceeding 6 mW from VCSELs with a shallow surface relief," *IEEE Photon. Technol. Lett.*, vol. 16, no. 2, pp. 368–370, 2004.

[2] D. Kuchta, A. V. Rylyakov, C. L. Schow, J. Proesel, C. Baks, P. Westbergh, J. S. Gustavsson, and A. Larsson, "64Gb/s Transmission over 57m MMF using an NRZ Modulated 850nm VCSEL," in *Optical Fiber Communication Conference (OFC)*, p. Th3C.2, 2014.

[3] P. Westbergh, J. S. Gustavsson, and A. Larsson, "VCSEL arrays for multicore fiber interconnects with an aggregate capacity of 240 Gb/s," *IEEE Photon. Technol. Lett.*, vol. 27, no. 3, pp. 296–299, 2015.

[4] H. Soda, K. Iga, C. Kitahara, and Y. Suematsu, "GaInAsP/InP surface emitting injection lasers," *Jap. J. Appl. Phys.*, vol. 18, no. 12, p. 2329, 1979.

[5] K. Iga, "Vertical-Cavity Surface-Emitting Laser: Its Conception and Evolution," *Jap. J. Appl. Phys.*, vol. 47, no. 1R, p. 1, 2008.

[6] I. Melngailis, "Longitudinal Injection-Plasma Laser of InSb," *Appl. Phys. Lett.*, vol. 6, no. 3, pp. 59–60, 1965.

[7] K. Takahashi, A. Yoshikawa, and A. Sandhu, *Wide bandgap semiconductors: fundamental properties and modern photonic and electronic devices*. Springer, 2007.

[8] T. Yokogawa, S. Yoshii, A. Tsujimura, Y. Sasai, and J. Merz, "Electrically pumped CdZnSe/ZnSe blue-green vertical-cavity surface-emitting lasers," *Jap. J. Appl. Phys.*, vol. 34, no. 6B, p. L751, 1995.

[9] H. Amano, M. Kito, K. Hiramatsu, and I. Akasaki, "P-type conduction in Mg-doped GaN treated with low-energy electron beam irradiation (LEEBI)," *Jap. J. Appl. Phys.*, vol. 28, no. 12A, p. L2112, 1989.

[10] S. Nakamura, T. Mukai, and M. Senoh, "High-power GaN pn junction blue-light-emitting diodes," *Jap. J. Appl. Phys.*, vol. 30, no. 12A, p. L1998, 1991.

[11] A. A. Bergh, "Blue laser diode (LD) and light emitting diode (LED) applications," *Phys. Stat. Sol. A*, vol. 201, no. 12, pp. 2740–2754, 2004.

[12] D. Feezell, "The evolving GaN VCSEL," *Compound Semiconductor*, vol. 20, no. 1, pp. 44–49, 2014.

[13] J. Hecht, "Photonic Frontiers: Nitride VCSELs: Nitride VCSELs pose a tough challenge," *Laser Focus World*, vol. 50, pp. 34–36, 2014.

[14] R. Shimada and H. Morkoc, "Wide Bandgap Semiconductor-Based Surface-Emitting Lasers: Recent Progress in GaN-Based Vertical Cavity Surface-Emitting Lasers and GaN-/ZnO-Based Polariton Lasers," *Proc. IEEE*, vol. 98, no. 7, pp. 1220–1233, 2010.

[15] Å. Haglund, E. Hashemi, J. Bengtsson, J. Gustavsson, M. Stattin, M. Calciati, and M. Goano, "Progress and challenges in electrically pumped GaN-based VCSELs," in *Proc. SPIE*, vol. 9892, pp. 98920Y–98920Y–20, 2016.

[16] D. F. Feezell, "Status and future of GaN-based vertical-cavity surface-emitting lasers," in *Proc. SPIE*, vol. 9363, pp. 93631G–93631G–13, 2015.

[17] C. Lee, C. Shen, H. M. Oubei, M. Cantore, B. Janjua, T. K. Ng, R. M. Farrell, M. M. El-Desouki, J. S. Speck, S. Nakamura, B. S. Ooi, and S. P. DenBaars, "2 Gbit/s data transmission from an unfiltered laser-based phosphor-converted white lighting communication system," *Opt. express*, vol. 23, no. 23, pp. 29779–29787, 2015.

[18] S. Watson, S. Viola, G. Giuliano, S. P. Najda, P. Perlin, T. Suski, L. Marona, M. Leszczynski, P. Wisniewski, R. Czernecki, G. Targowski, M. A. Watson, H. White, D. Rowe, L. Laycock, and A. E. Kelly, "High speed visible light communication using blue GaN laser diodes," in *Proc. SPIE*, vol. 9991, pp. 99910A–99910A–7, 2016.

[19] J. J. McKendry, D. Massoubre, S. Zhang, B. R. Rae, R. P. Green, E. Gu, R. K. Henderson, A. Kelly, and M. D. Dawson, "Visible-light communications using a CMOS-controlled micro-light-emitting-diode array," *J. Lightw. Technol.*, vol. 30, no. 1, pp. 61–67, 2012.

[20] J. J. McKendry, R. P. Green, A. Kelly, Z. Gong, B. Guilhabert, D. Massoubre, E. Gu, and M. D. Dawson, "High-speed visible light communications using individual pixels in a micro light-emitting diode array," *IEEE Photon. Technol. Lett.*, vol. 22, no. 18, pp. 1346–1348, 2010.

[21] C. Lee, C. Zhang, M. Cantore, R. M. Farrell, S. H. Oh, T. Margalith, J. S. Speck, S. Nakamura, J. E. Bowers, and S. P. DenBaars, "4 Gbps direct modulation of 450 nm GaN laser for high-speed visible light communication," *Opt. express*, vol. 23, no. 12, pp. 16232–16237, 2015.

[22] Y. C. Chi, D. H. Hsieh, C. T. Tsai, H. Y. Chen, H. C. Kuo, and G. R. Lin, "450-nm GaN laser diode enables high-speed visible light communication with 9-Gbps QAM-OFDM," *Opt. express*, vol. 23, no. 10, pp. 13051–13059, 2015.

[23] C. Shen, J. T. Leonard, E. C. Young, T. K. Ng, S. P. DenBaars, J. S. Speck, S. Nakamura, A. Y. Alyamani, M. M. El-Desouki, and B. S. Ooi, "GHz modulation bandwidth from single-longitudinal mode violet-blue VCSEL using nonpolar InGaN/GaN QWs," in *Conference on Lasers and Electro-Optics*, p. STh1L.2, Optical Society of America, 2016.

[24] R. Stevenson, "Solid-State Lighting: Are Laser Diodes The Logical Successors To LEDs?," *Compound Semiconductor*, vol. 19, no. 8, pp. 40–44, 2013.

[25] J. Y. Tsao, M. H. Crawford, M. E. Coltrin, A. J. Fischer, D. D. Koleske, G. S. Subramania, G. Wang, J. J. Wierer, and R. F. Karlicek, "Toward Smart and Ultra-efficient Solid-State Lighting," *Adv. Opt. Mat.*, vol. 2, no. 9, pp. 809–836, 2014.

[26] J. Iveland, L. Martinelli, J. Peretti, J. S. Speck, and C. Weisbuch, "Direct Measurement of Auger Electrons Emitted from a Semiconductor Light-Emitting Diode under Electrical Injection: Identification of the Dominant Mechanism for Efficiency Droop," *Phys. Rev. Lett.*, vol. 110, p. 177406, Apr 2013.

[27] L. Y. Kuritzky and J. S. Speck, "Lighting for the 21st century with laser diodes based on non-basal plane orientations of GaN," *MRS Communications*, vol. 5, no. 03, pp. 463–473, 2015.

[28] J. J. Wierer and J. Y. Tsao, "Advantages of III-nitride laser diodes in solid-state lighting," *Phys. Stat. Sol. A*, vol. 212, no. 5, pp. 980–985, 2015.

[29] N. Chi, Y. Wang, Y. Wang, X. Huang, and X. Lu, "Ultra-high-speed single red-green-blue light-emitting diode-based visible light communication systemutilizing advanced modulation formats," *Chin. Opt. Lett.*, vol. 12, p. 010605, Jan 2014.

[30] R. R. Hainich and O. Bimber, *Displays: fundamentals and applications*. CRC press, 2016.

[31] M. T. Hardy, D. F. Feezell, S. P. DenBaars, and S. Nakamura, "Group III-nitride lasers: a materials perspective," *Materials Today*, vol. 14, no. 9, pp. 408–415, 2011.

[32] U. Strauβ, S. Brüninghoff, M. Schillgalies, C. Vierheilig, N. Gmeinwieser, V. Kümmler, G. Brüderl, S. Lutgen, A. Avramescu, D. Queren, *et al.*, "True-blue InGaN laser for pico size projectors," in *Proc. SPIE, Gallium Nitride Materials and Devices III*, vol. 689417, International Society for Optics and Photonics, 2008.

[33] C. Greb, "Fluorescent Dyes: An Overview," 2012.

[34] M. Panjehpour, C. E. Julius, M. N. Phan, T. Vo-Dinh, and S. Overholt, "Laser-induced fluorescence spectroscopy for in vivo diagnosis of non-melanoma skin cancers," *Lasers in surgery and medicine*, vol. 31, no. 5, pp. 367–373, 2002.

[35] T. Vo-Dinh, M. Panjehpour, B. F. Overholt, C. Farris, F. P. Buckley, and R. Sneed, "In vivo cancer diagnosis of the esophagus using differential normalized fluorescence (DNF) indices," *Lasers in surgery and medicine*, vol. 16, no. 1, pp. 41–47, 1995.

[36] A. Llobera, J. Juvert, A. González-Fernández, B. Ibarlucea, E. Carregal-Romero, S. Büttgenbach, and C. Fernández-Sánchez, "Biofunctionalized all-polymer photonic lab on a chip with integrated solid-state light emitter," *Light Sci. Appl.*, vol. 4, no. 4, p. e271, 2015.

[37] H. Morkoç, *Handbook of Nitride Semiconductors and Devices, Materials Properties, Physics and Growth*, vol. 1. John Wiley & Sons, 2009.

[38] T. Lei, M. Fanciulli, R. Molnar, T. Moustakas, R. Graham, and J. Scanlon, "Epitaxial growth of zinc blende and wurtzitic gallium nitride thin films on (001) silicon," *Appl. Phys. Lett.*, vol. 59, no. 8, pp. 944–946, 1991.

[39] M. Paisley, Z. Sitar, J. Posthill, and R. Davis, "Growth of cubic phase gallium nitride by modified molecular-beam epitaxy," *J. Vac. Sci. Technol. A*, vol. 7, no. 3, pp. 701–705, 1989.

[40] M. Mizuta, S. Fujieda, Y. Matsumoto, and T. Kawamura, "Low temperature growth of GaN and AlN on GaAs utilizing metalorganics and hydrazine," *Jap. J. Appl. Phys.*, vol. 25, no. 12A, p. L945, 1986.

[41] M. Stutzmann, O. Ambacher, M. Eickhoff, U. Karrer, A. Lima Pimenta, R. Neuberger, J. Schalwig, R. Dimitrov, P. Schuck, and R. Grober, "Playing with polarity," *Phys. Stat. Sol. B*, vol. 228, no. 2, pp. 505–512, 2001.

[42] O. Ambacher, J. Smart, J. Shealy, N. Weimann, K. Chu, M. Murphy, W. Schaff, L. Eastman, R. Dimitrov, L. Wittmer, *et al.*, "Two-dimensional electron gases induced by spontaneous and piezoelectric polarization charges in N-and Ga-face AlGaN/GaN heterostructures," *J. Appl. Phys.*, vol. 85, no. 6, pp. 3222–3233, 1999.

[43] G. Rossbach, *High-Density Excitonic Effects in GaN*. PhD thesis, EPFL, 2014.

[44] G. Rossbach, M. Röppischer, P. Schley, G. Gobsch, C. Werner, C. Cobet, N. Esser, A. Dadgar, M. Wieneke, A. Krost, *et al.*, "Valence-band splitting and optical anisotropy of AlN," *Phys. Stat. Sol. B*, vol. 247, no. 7, pp. 1679–1682, 2010.

[45] R. Goldhahn, C. Buchheim, P. Schley, A. T. Winzer, and H. Wenzel, "Optical constants of bulk nitrides," in *Nitride Semiconductor Devices: Principles and Simulation* (J. Piprek, ed.), Wiley-VCH, 2007.

[46] J. Piprek, R. Farrell, S. DenBaars, and S. Nakamura, "Effects of built-in polarization on InGaN-GaN vertical-cavity surface-emitting lasers," *IEEE Photon. Technol. Lett.*, vol. 18, no. 1, pp. 7–9, 2006.

[47] U. Strauß, A. Avramescu, T. Lermer, D. Queren, A. Gomez-Iglesias, C. Eichler, J. Müller, G. Brüderl, and S. Lutgen, "Pros and cons of green InGaN laser on c-plane GaN," *Phys. Stat. Sol. B*, vol. 248, no. 3, pp. 652–657, 2011.

[48] D. Sizov, R. Bhat, and C.-E. Zah, "Gallium indium nitride-based green lasers," *J. Lightw. Technol.*, vol. 30, no. 5, pp. 679–699, 2012.

[49] F. Della Sala, A. Di Carlo, P. Lugli, F. Bernardini, V. Fiorentini, R. Scholz, and J.-M. Jancu, "Free-carrier screening of polarization fields in wurtzite GaN/InGaN laser structures," *Appl. Phys. Lett.*, vol. 74, no. 14, pp. 2002–2004, 1999.

[50] G. Zhang, Y. Tong, Z. Yang, S. Jin, J. Li, and Z. Gan, "Relationship of background carrier concentration and defects in GaN grown by metalorganic vapor phase epitaxy," *Appl. Phys. Lett.*, vol. 71, no. 23, pp. 3376–3378, 1997.

[51] J. Jayapalan, B. Skromme, R. Vaudo, and V. Phanse, "Optical spectroscopy of Si-related donor and acceptor levels in Si-doped GaN grown by hydride vapor phase epitaxy," *Appl. Phys. Lett.*, vol. 73, no. 9, pp. 1188–1190, 1998.

[52] W. Götz, N. Johnson, J. Walker, D. Bour, and R. Street, "Activation of acceptors in Mg-doped GaN grown by metalorganic chemical vapor deposition," *Appl. Phys. Lett.*, vol. 68, no. 5, pp. 667–669, 1996.

[53] S. Nakamura, M. Senoh, S.-i. Nagahama, N. Iwasa, T. Yamada, T. Matsushita, Y. Sugimoto, and H. Kiyoku, "Room-temperature continuous-wave operation of InGaN multi-quantum-well structure laser diodes," *Appl. Phys. Lett.*, vol. 69, no. 26, pp. 4056–4058, 1996.

[54] M. Kneissl and J. Rass, "Laser diodes in the visible spectral range:GaN-based blue and green laser diodes," in *Laser Systems* (H. Weber, P. Loosen, and R. Poprawe, eds.), vol. 3 of *Landolt-Börnstein - Group VIII Advanced Materials and Technologies*, pp. 22–37, Springer Berlin Heidelberg, 2011.

[55] S. C. Wang, T. C. Lu, C. C. Kao, J. T. Chu, G. S. Huang, H. C. Kuo, S. W. Chen, T. T. Kao, J. R. Chen, and L. F. Lin, "Optically pumped GaN-based vertical cavity surface emitting lasers: technology and characteristics," *Jap. J. Appl. Phys.*, vol. 46, no. 8S, p. 5397, 2007.

[56] E. Feltin, G. Christmann, J. Dorsaz, A. Castiglia, J.-F. Carlin, R. Butté, N. Grandjean, S. Christopoulos, G. B. H. von Högersthal, A. Grundy, *et al.*, "Blue lasing at room temperature in an optically pumped lattice-matched AlInN/GaN VCSEL structure," *Electron. Lett.*, vol. 43, no. 17, pp. 924–926, 2007.

[57] P. Mackowiak and W. Nakwaski, "Some aspects of designing an efficient nitride VCSEL resonator," *J. Phys. D: Appl. Phys.*, vol. 34, no. 6, p. 954, 2001.

[58] P. Mackowiak, R. P. Sarzala, M. Wasiak, and W. Nakwaski, "Design guidelines for fundamental-mode-operated cascade nitride VCSELs," *IEEE Photon. Technol. Lett.*, vol. 15, no. 4, pp. 495–497, 2003.

[59] T. C. Lu, C. C. Kao, H. C. Kuo, G. S. Huang, and S. C. Wang, "CW lasing of current injection blue GaN-based vertical cavity surface emitting laser," *Appl. Phys. Lett.*, vol. 92, no. 14, p. 141102, 2008.

[60] Y. Higuchi, K. Omae, H. Matsumura, and T. Mukai, "Room-temperature CW lasing of a GaN-based vertical-cavity surface-emitting laser by current injection," *Appl. Phys. Expr.*, vol. 1, no. 12, p. 121102, 2008.

[61] T. C. Lu, S. W. Chen, T. T. Wu, P. M. Tu, C. K. Chen, C. H. Chen, Z. Y. Li, H. C. Kuo, and S. C. Wang, "Continuous wave operation of current injected GaN vertical cavity surface emitting lasers at room temperature," *Appl. Phys. Lett.*, vol. 97, no. 7, p. 071114, 2010.

[62] G. Cosendey, A. Castiglia, G. Rossbach, J.-F. Carlin, and N. Grandjean, "Blue monolithic AlInN-based vertical cavity surface emitting laser diode on free-standing GaN substrate," *Appl. Phys. Lett.*, vol. 101, no. 15, p. 151113, 2012.

[63] T. Furuta, K. Matsui, K. Horikawa, K. Ikeyama, Y. Kozuka, S. Yoshida, T. Akagi, T. Takeuchi, S. Kamiyama, M. Iwaya, and I. Akasaki, "Room-temperature CW operation of a nitride-based vertical-cavity surface-emitting laser using thick GaInN quantum wells," *Jap. J. Appl. Phys.*, vol. 55, no. 5S, p. 05FJ11, 2016.

[64] D. Kasahara, D. Morita, T. Kosugi, K. Nakagawa, J. Kawamata, Y. Higuchi, H. Matsumura, and T. Mukai, "Demonstration of blue and green GaN-based vertical-cavity surface-emitting lasers by current injection at room temperature," *Appl. Phys. Express*, vol. 4, no. 7, p. 072103, 2011.

[65] T. Onishi, O. Imafuji, K. Nagamatsu, M. Kawaguchi, K. Yamanaka, and S. Takigawa, "Continuous wave operation of GaN vertical cavity surface emitting lasers at room temperature," *IEEE J. Quantum Electron.*, vol. 48, no. 9, pp. 1107–1112, 2012.

[66] W.-J. Liu, X.-L. Hu, L. Y. Ying, J.-Y. Zhang, and B.-P. Zhang, "Room temperature continuous wave lasing of electrically injected GaN-based vertical cavity surface emitting lasers," *Appl. Phys. Lett.*, vol. 104, no. 25, p. 251116, 2014.

[67] C. O. Holder, J. T. Leonard, R. M. Farrell, D. A. Cohen, B. P. Yonkee, J. S. Speck, S. P. DenBaars, S. Nakamura, and D. F. Feezell, "Nonpolar III-nitride vertical-cavity surface emitting lasers with a polarization ratio of 100 percent fabricated using photoelectrochemical etching," *Appl. Phys. Lett.*, vol. 105, no. 3, p. 031111, 2014.

[68] S. Izumi, N. Fuutagawa, T. Hamaguchi, M. Murayama, M. Kuramoto, and H. Narui, "Room-temperature continuous-wave operation of GaN-based vertical-cavity surface-emitting lasers fabricated using epitaxial lateral overgrowth," *Appl. Phys. Express*, vol. 8, no. 6, p. 062702, 2015.

[69] K. Ikeyama, Y. Kozuka, K. Matsui, S. Yoshida, T. Akagi, Y. Akatsuka, N. Koide, T. Takeuchi, S. Kamiyama, M. Iwaya, and I. Akasaki, "Room-temperature continuous-wave operation of GaN-based vertical-cavity surface-emitting lasers with n-type conducting AlInN/GaN distributed bragg reflectors," *Appl. Phys. Express*, vol. 9, no. 10, p. 102101, 2016.

[70] D. H. Hsieh, A. J. Tzou, T. S. Kao, F. I. Lai, D. W. Lin, B. C. Lin, T. C. Lu, W. C. Lai, C. H. Chen, and H. C. Kuo, "Improved carrier injection in GaN-based VCSEL via AlGaN/GaN multiple quantum barrier electron blocking layer," *Opt. express*, vol. 23, no. 21, pp. 27145–27151, 2015.

[71] M. K., F. T., H. N., K. Y., A. T., T. T., K. S., I. M., and A. I., "3-mW RT-CW GaN-Based VCSELs and Their Temperature Dependence." presented at the International Workshop on Nitride Semiconductors, Orlando, USA, October 2016.

[72] T. Hamaguchi, N. Fuutagawa, S. Izumi, M. Murayama, and H. Narui, "Milliwatt-class GaN-based blue vertical-cavity surface-emitting lasers fabricated by epitaxial lateral overgrowth," *Phys. Status Solidi A*, vol. 213, no. 5, pp. 1170–1176, 2016.

[73] K. Omae, Y. Higuchi, K. Nakagawa, H. Matsumura, and T. Mukai, "Improvement in lasing characteristics of GaN-based vertical-cavity surface-emitting lasers fabricated using a GaN substrate," *Appl. Phys. Express*, vol. 2, no. 5, p. 052101, 2009.

[74] C. Holder, J. S. Speck, S. P. DenBaars, S. Nakamura, and D. Feezell, "Demonstration of Nonpolar GaN-Based Vertical-Cavity Surface-Emitting Lasers," *Appl. Phys. Express*, vol. 5, no. 9, p. 092104, 2012.

[75] B. C. Lin, Y. A. Chang, K. J. Chen, C. H. Chiu, Z. Y. Li, Y. P. Lan, C. C. Lin, P. T. Lee, Y. K. Kuo, M. H. Shih, *et al.*, "Design and fabrication of a InGaN vertical-cavity surface-emitting laser with a composition-graded electron-blocking layer," *Laser Phys. Lett.*, vol. 11, no. 8, p. 085002, 2014.

[76] J. T. Leonard, D. A. Cohen, B. P. Yonkee, R. M. Farrell, T. Margalith, S. Lee, S. P. DenBaars, J. S. Speck, and S. Nakamura, "Nonpolar III-nitride vertical-cavity surface-emitting lasers incorporating an ion implanted aperture," *Appl. Phys. Lett.*, vol. 107, no. 1, p. 011102, 2015.

[77] J. T. Leonard, E. C. Young, B. P. Yonkee, D. A. Cohen, T. Margalith, S. P. DenBaars, J. S. Speck, and S. Nakamura, "Demonstration of a III-nitride vertical-cavity surface-emitting laser with a III-nitride tunnel junction intracavity contact," *Appl. Phys. Lett.*, vol. 107, no. 9, p. 091105, 2015.

[78] J. Leonard, B. Yonkee, D. Cohen, L. Megalini, S. Lee, J. Speck, S. DenBaars, and S. Nakamura, "Nonpolar III-nitride vertical-cavity surface-emitting laser with a photoelectrochemically etched air-gap aperture," *Appl. Phys. Lett.*, vol. 108, no. 3, p. 031111, 2016.

[79] K. Matsui, Y. Kozuka, K. Ikeyama, K. Horikawa, T. Furuta, T. Akagi, T. Takeuchi, S. Kamiyama, M. Iwaya, and I. Akasaki, "Gan-based vertical cavity surface emitting lasers with periodic gain structures," *Jap. J. Appl. Phys.*, vol. 55, no. 5S, p. 05FJ08, 2016.

[80] T. C. Lu, J. R. Chen, S. W. Chen, H. C. Kuo, C. C. Kuo, C. C. Lee, and S. C. Wang, "Development of GaN-based Vertical-cavity Surface-emitting Lasers," *IEEE J. Sel. Top. Quantum Electron.*, vol. 15, no. 3, pp. 850–860, 2009.

[81] G. Cosendey, J.-F. Carlin, N. A. Kaufmann, R. Butté, and N. Grandjean, "Strain compensation in AlInN/GaN multilayers on GaN substrates: Application to the realization of defect-free Bragg reflectors," *Appl. Phys. Lett.*, vol. 98, no. 18, p. 181111, 2011.

[82] T. Ueda, M. Ishida, and M. Yuri, "Separation of thin GaN from sapphire by laser lift-off technique," *Jap. J. Appl. Phys*, vol. 50, no. 4R, p. 041001, 2011.

[83] J. Piprek, "What is the problem with GaN-based VCSELs?," in *Numerical Simulation of Optoelectronic Devices (NUSOD), 2013 13th International Conference on*, pp. 89–90, IEEE, 2013.

[84] J. S. Gustavsson, J. A. Vukusic, J. Bengtsson, and A. Larsson, "A comprehensive model for the modal dynamics of vertical-cavity surface-emitting lasers," *IEEE J. Quantum Electron.*, vol. 38, no. 2, pp. 203–212, 2002.

[85] J. Piprek, R. Farrell, S. DenBaars, and S. Nakamura, "Effects of built-in polarization on InGaN-GaN vertical-cavity surface-emitting lasers," *IEEE Photon. Technol. Lett.*, vol. 18, no. 1, pp. 7–9, 2006.

[86] B. C. Lin, Y. A. Chang, K. J. Chen, C. H. Chiu, Z. Y. Li, Y. P. Lan, C. C. Lin, P. T. Lee, Y. K. Kuo, M. H. Shih, *et al.*, "Design and fabrication of a InGaN vertical-cavity surface-emitting laser with a composition-graded electron-blocking layer," *Laser Phys. Lett.*, vol. 11, no. 8, p. 085002, 2014.

[87] D. Hsieh, A. Tzou, T. Kao, F. Lai, D. Lin, B. Lin, T. Lu, W. Lai, C. Chen, and H. Kuo, "Improved carrier injection in GaN-based VCSEL via AlGaN/GaN multiple quantum barrier electron blocking layer," *Opt. express*, vol. 23, no. 21, pp. 27145–27151, 2015.

[88] A. David, M. J. Grundmann, J. F. Kaeding, N. F. Gardner, T. G. Mihopoulos, and M. R. Krames, "Carrier distribution in (0001) InGaN/GaN multiple quantum well light-emitting diodes," *Appl. Phys. Lett.*, vol. 92, no. 5, p. 053502, 2008.

[89] J. Piprek, "Gan-based vertical-cavity laser performance improvements using tunnel-junction-cascaded active regions," *Appl. Phys. Lett.*, vol. 105, no. 1, p. 011116, 2014.

[90] W. Scheibenzuber, U. Schwarz, R. Veprek, B. Witzigmann, and A. Hangleiter, "Calculation of optical eigenmodes and gain in semipolar and nonpolar InGaN/GaN laser diodes," *Phys. Rev. B*, vol. 80, no. 11, p. 115320, 2009.

[91] K. K. Kim, H. Kim, S. N. Lee, and S. Cho, "Structural, optical, and electrical properties of E-beam and sputter-deposited ITO films for LED applications," *Electron. Mat. Lett.*, vol. 7, no. 2, pp. 145–149, 2011.

[92] S. J. Chang, C. Lan, J. D. Hwang, Y. Cheng, W. Lin, J. Lin, and H. Z. Chen, "Sputtered indium-tin-oxide on p-GaN," *J. Electrochemical Soc.*, vol. 155, no. 2, pp. H140–H143, 2008.

[93] E. P. Systems, "LEDs & OLEDs." Online: `http://www.evatecnet.com/markets/optoelectronics/leds/leds-and-oleds-brochure`, July 2012. Last checked: 2014-12-28.

[94] S. S. Thöny, H. Friedli, M. Padrun, A. Castiglia, G. Cosendey, and N. Grandjean, "Damage-free ITO deposition on LED devices," in *IWN2012 - International Workshop on Nitride Semiconductors - Abstract Book*, pp. ThP–OD.20, 2012.

[95] J. Leonard, D. Cohen, B. Yonkee, R. Farrell, S. DenBaars, J. Speck, and S. Nakamura, "Smooth e-beam-deposited tin-doped indium oxide for III-nitride vertical-cavity surface-emitting laser intracavity contacts," *J. Appl. Phys.*, vol. 118, no. 14, p. 145304, 2015.

[96] M. Oh, W. Y. Jin, H. J. Jeong, M. S. Jeong, J. W. Kang, and H. Kim, "Silver nanowire transparent conductive electrodes for high-efficiency III-nitride light-emitting diodes," *Sci. Rep.*, vol. 5, 2015.

[97] M. Stattin, C. J. Lockhart de la Rosa, J. Sun, A. Yurgens, and Å. Haglund, "Metal-Free Graphene as Transparent Electrode for GaN-Based Light-Emitters," *Jap. J. Appl. Phys.*, vol. 52, 2013.

[98] T. Minami, "Transparent conducting oxide semiconductors for transparent electrodes," *Semicond. Sci. Technol.*, vol. 20, no. 4, p. S35, 2005.

[99] J. Sheu, Y.-K. Su, G.-C. Chi, P. Koh, M. Jou, C. Chang, C. Liu, and W. Hung, "High-transparency Ni/Au ohmic contact to p-type GaN," *Appl. Phys. Lett.*, vol. 74, no. 16, pp. 2340–2342, 1999.

[100] D. Feezell, R. Farrell, M. Schmidt, H. Yamada, M. Ishida, S. Denbaars, D. Cohen, and S. Nakamura, "Thin metal intra-cavity contact and lateral current-distribution scheme for GaN-based vertical-cavity lasers," in *APS Meeting Abstracts*, vol. 1, p. 41012, 2007.

[101] G. Kästle, H.-G. Boyen, A. Schröder, A. Plettl, and P. Ziemann, "Size effect of the resistivity of thin epitaxial gold films," *Phys. Rev. B*, vol. 70, no. 16, p. 165414, 2004.

[102] C. J. L. de la Rosa, J. Sun, N. Lindvall, M. T. Cole, Y. Nam, M. Löffler, E. Olsson, K. B. Teo, and A. Yurgens, "Frame assisted H2O electrolysis induced H2 bubbling transfer of large area graphene grown by chemical vapor deposition on Cu," *Appl. Phys. Lett.*, vol. 102, no. 2, p. 022101, 2013.

[103] J. Sun, M. T. Cole, S. A. Ahmad, O. Backe, T. Ive, M. Loffler, N. Lindvall, E. Olsson, K. B. Teo, J. Liu, *et al.*, "Direct chemical vapor deposition of large-area carbon thin films on gallium nitride for transparent electrodes: a first attempt," *IEEE Trans. Semicond. Manuf.*, vol. 25, no. 3, pp. 494–501, 2012.

[104] Y. S. Kim, K. Joo, S.-K. Jerng, J. H. Lee, D. Moon, J. Kim, E. Yoon, and S.-H. Chun, "Direct integration of polycrystalline graphene into light emitting diodes by plasma-assisted metal-catalyst-free synthesis," *ACS Nano*, vol. 8, no. 3, pp. 2230–2236, 2014.

[105] M. Ortsiefer, W. Hofmann, J. Rosskopf, and M.-C. Amann, "Long-Wavelength VCSELs with Buried Tunnel Junction," in *VCSELs*, pp. 321–351, Springer, 2013.

[106] S. Nakamura, "The Roles of Structural Imperfections in InGaN-based Blue Light-Emitting Diodes and Laser Diodes," *Science*, vol. 281, no. 5379, pp. 956–961, 1998.

[107] D. T. S. Watson-Parris, *Carrier localization in InGaN/GaN quantum wells.* PhD thesis, University of Manchester, 2011.

[108] B. S. Cheng, Y. L. Wu, T. C. Lu, C. H. Chiu, C. H. Chen, P. M. Tu, H. C. Kuo, S. C. Wang, and C. Y. Chang, "High Q microcavity light emitting diodes with buried AlN current apertures," *Appl. Phys. Lett.*, vol. 99, no. 4, p. 041101, 2011.

[109] M. Ohya, K. Fukuda, I. Masumoto, S. Kohmoto, K. Naniwae, M. Yamada, M. Matsudate, T. Tsukuda, T. Akagawa, and C. Sasaoka, "High-power operation of inner-stripe GaN-based blue-violet laser diodes," vol. 6485, pp. 648505–648505–9, 2007.

[110] W.-S. Tan, K. Takahashi, V. Bousquet, A. Ariyoshi, Y. Tsuda, M. Ohta, and M. Kauer, "Blue-violet inner stripe laser diodes using lattice matched AlInN as current confinement layer for high power operation," *Appl. Phys. Express*, vol. 2, no. 11, p. 112101, 2009.

[111] A. Castiglia, D. Simeonov, H. Buehlmann, J.-F. Carlin, E. Feltin, J. Dorsaz, R. Butté, and N. Grandjean, "Efficient current injection scheme for nitride vertical cavity surface emitting lasers," *Appl. Phys. Lett.*, vol. 90, no. 3, pp. 033514–033514, 2007.

[112] v. n. p. y. p. Jörgen Bengtsson and Johan Gustavsson and Å sa Haglund and Anders Larsson and Alexander Bachmann and Kaveh Kashani-Shirazi and Markus-Christian Amann, journal=Opt. Express, "Diffraction loss in long-wavelength buried tunnel junction VCSELs analyzed with a hybrid coupled-cavity transfer-matrix model,"

[113] R. Safaisini, E. Haglund, P. Westbergh, J. S. Gustavsson, and A. Larsson, "20 Gbit/s data transmission over 2 km multimode fibre using 850 nm mode filter VCSEL," *Electron. Lett.*, vol. 50, no. 1, p. 40, 2014.

[114] Y. Y. Lai, S. C. Huang, T. L. Ho, T. C. Lu, and S. C. Wang, "Numerical analysis on current and optical confinement of III-nitride vertical-cavity surface-emitting lasers," *Opt. express*, vol. 22, no. 8, pp. 9789–9797, 2014.

[115] T. Hamaguchi, H. Nakajima, M. Ito, J. Mitomo, S. Satou, N. Fuutagawa, and H. Narui, "Lateral carrier confinement of GaN-based vertical-cavity surface-emitting diodes using boron ion implantation," *Jap. J. Appl. Phys.*, vol. 55, no. 12, p. 122101, 2016.

[116] C. Berger, A. Lesnik, T. Zettler, G. Schmidt, P. Veit, A. Dadgar, J. Bläsing, J. Christen, and A. Strittmatter, "Metalorganic chemical vapor phase epitaxy of narrow-band distributed bragg reflectors realized by GaN: Ge modulation doping," *J. Crys. Growth*, vol. 440, pp. 6–12, 2016.

[117] Y. Kozuka, K. Ikeyama, T. Yasuda, T. Takeuchi, S. Kamiyama, M. Iwaya, and I. Akasaki, "Growths of AlInN Single Layers and Distributed Bragg Reflectors for VCSELs," in *MRS Proc.*, vol. 1736, pp. mrsf14–1736, Cambridge Univ Press, 2015.

[118] N. Nakada, H. Ishikawa, T. Egawa, and T. Jimbo, "Suppression of crack generation in GaN/AlGaN distributed bragg reflector on sapphire by the insertion of GaN/AlGaN superlattice grown by Metal-organic Chemical Vapor Deposition," *Jap. J. Appl. Phys.*, vol. 42, no. 2B, p. L144, 2003.

[119] G. S. Huang, T. C. Lu, H. H. Yao, H. C. Kuo, S. C. Wang, C.-W. Lin, and L. Chang, "Crack-free GaN/AlN distributed bragg reflectors incorporated with GaN/AlN superlattices grown by metalorganic chemical vapor deposition," *Appl. Phys. Lett.*, vol. 88, no. 6, p. 061904, 2006.

[120] K. Waldrip, J. Han, J. J. Figiel, H. Zhou, E. Makarona, and A. Nurmikko, "Stress engineering during metalorganic chemical vapor deposition of AlGaN/GaN distributed Bragg reflectors," *Appl. Phys. Lett.*, vol. 78, no. 21, pp. 3205–3207, 2001.

[121] Ž. Gačević, A. Eljarrat, F. Peiró, and E. Calleja, "Insight into high-reflectivity AlN/GaN Bragg reflectors with spontaneously formed (Al, Ga)N transient layers at the interfaces," *J. Appl. Phys.*, vol. 113, no. 18, p. 183106, 2013.

[122] T. Ive, O. Brandt, H. Kostial, T. Hesjedal, M. Ramsteiner, and K. H. Ploog, "Crack-free and conductive Si-doped AlN/GaN distributed Bragg reflectors grown on 6H-SiC(0001)," *Appl. Phys. Lett.*, vol. 85, no. 11, pp. 1970–1972, 2004.

[123] K. Yagi, M. Kaga, K. Yamashita, K. Takeda, M. Iwaya, T. Takeuchi, S. Kamiyama, H. Amano, and I. Akasaki, "Crack-free AlN/GaN Distributed Bragg Reflectors on AlN Templates," *Jap. J. Appl. Phys.*, vol. 51, no. 5R, p. 051001, 2012.

[124] X. Ni, R. Shimada, T. Kang, J. Leach, Ü. Özgür, and H. Morkoç, "Gan-based vertical cavities with crack-free high-reflectivity patterned AlGaN/GaN distributed Bragg reflectors," *Phys. Stat. Sol. A*, vol. 206, no. 2, pp. 367–370, 2009.

[125] M. Arita, M. Nishioka, and Y. Arakawa, "InGaN Vertical Microcavity LEDs with a Si-Doped AlGaN/GaN Distributed Bragg Reflector," *Phys. Stat. Sol. A*, vol. 194, no. 2, pp. 403–406, 2002.

[126] S. Figge, H. Dartsch, T. Aschenbrenner, C. Kruse, and D. Hommel, "Distributed Bragg reflectors in comparison to RUGATE and nested super lattices-growth, reflectivity, and conductivity," *Phys. Stat. Sol. C*, vol. 5, no. 6, pp. 1839–1842, 2008.

[127] T. Ive, O. Brandt, H. Kostial, T. Hesjedal, M. Ramsteiner, and K. H. Ploog, "Crack-free and conductive Si-doped AlN/GaN distributed bragg reflectors grown on 6h-sic (0001)," *Appl. Phys. Lett.*, vol. 85, no. 11, pp. 1970–1972, 2004.

[128] Y. S. Liu, A. S. Haq, T. T. Kao, K. Mehta, S. C. Shen, T. Detchprohm, P. D. Yoder, R. D. Dupuis, H. Xie, and F. A. Ponce, "Electrically conducting n-type AlGaN/GaN distributed Bragg reflectors grown by metalorganic chemical vapor deposition," *J. Crys. Growth*, vol. 443, pp. 81–84, 2016.

[129] S. Yoshida, K. Ikeyama, T. Yasuda, T. Furuta, T. Takeuchi, M. Iwaya, S. Kamiyama, and I. Akasaki, "Electron and hole accumulations at GaN/AlInN/GaN interfaces and conductive n-type AlInN/GaN distributed Bragg reflectors," *Jap. J. Appl. Phys.*, vol. 55, no. 5S, p. 05FD10, 2016.

[130] R. Andersson, "Investigation of electrical contacts on n-type 4H-SiC," master's thesis, Chalmers University of Technology, Photonics Laboratory SE-41296 Gothenburg, 2015.

[131] F. Hjort, "Electrical conductivity of n-doped GaN-based distributed Bragg reflectors," master's thesis, Chalmers University of Technology, Photonics Laboratory SE-41296 Gothenburg, 2016.

[132] L. Carletti, R. Malureanu, J. Mørk, and I.-S. Chung, "High-index-contrast grating reflector with beam steering ability for the transmitted beam," *Opt. express*, vol. 19, no. 23, pp. 23567–23572, 2011.

[133] D. Fattal, J. Li, Z. Peng, M. Fiorentino, and R. G. Beausoleil, "Flat dielectric grating reflectors with focusing abilities," *Nat. Photonics*, vol. 4, no. 7, pp. 466–470, 2010.

[134] V. Karagodsky, C. Chase, and C. J. Chang-Hasnain, "Matrix Fabry-Perot resonance mechanism in high-contrast gratings," *Opt. lett.*, vol. 36, no. 9, pp. 1704–1706, 2011.

[135] C. J. Chang-Hasnain and W. Yang, "High-contrast gratings for integrated optoelectronics," *Adv. Opt. Photon.*, vol. 4, no. 3, pp. 379–440, 2012.

[136] M. C. Huang, Y. Zhou, and C. J. Chang-Hasnain, "A surface-emitting laser incorporating a high-index-contrast subwavelength grating," *Nat. Photonics*, vol. 1, no. 2, pp. 119–122, 2007.

[137] P. Gilet, N. Olivier, P. Grosse, K. Gilbert, A. Chelnokov, I.-S. Chung, and J. Mørk, "High-index-contrast subwavelength grating VCSEL," vol. 7615, pp. 76150J–76150J–8, 2010.

[138] C. Chase, Y. Rao, W. Hofmann, and C. J. Chang-Hasnain, "1550 nm high contrast grating VCSEL," *Opt. express*, vol. 18, no. 15, pp. 15461–15466, 2010.

[139] E. Haglund, J. S. Gustavsson, J. Bengtsson, Å. Haglund, A. Larsson, D. Fattal, W. Sorin, and M. Tan, "Demonstration of post-growth wavelength setting of VCSELs using high-contrast gratings," *Opt. express*, vol. 24, no. 3, pp. 1999–2005, 2016.

[140] T. Ansbæk, I.-S. Chung, E. S. Semenova, and K. Yvind, "1060-nm tunable Monolithic High Index Contrast Subwavelength Grating VCSEL," *IEEE Photon. Technol. Lett.*, vol. 25, no. 4, pp. 365–367, 2013.

[141] W. Hofmann, C. Chase, M. Muller, Y. Rao, C. Grasse, G. Boĺhm, M.-C. Amann, and C. J. Chang-Hasnain, "Long-wavelength high-contrast grating vertical-cavity surface-emitting laser," *IEEE Photon. J.*, vol. 2, no. 3, pp. 415–422, 2010.

[142] C. Sciancalepore, B. B. Bakir, S. Menezo, X. Letartre, D. Bordel, and P. Viktorovitch, "III-V-on-Si Photonic Crystal Vertical-Cavity Surface-Emitting Laser Arrays for Wavelength Division Multiplexing," *IEEE Photon. Technol. Lett.*, vol. 25, no. 12, pp. 1111–1113, 2013.

[143] J. Kim, D. U. Kim, J. Lee, H. Jeon, Y. Park, and Y. S. Choi, "AlGaN membrane grating reflector," *Appl. Phys. Lett.*, vol. 95, no. 2, p. 021102, 2009.

[144] T. T. Wu, Y. C. Syu, S. H. Wu, W. T. Chen, T. C. Lu, S. C. Wang, H. P. Chiang, and D. P. Tsai, "Sub-wavelength GaN-based membrane high contrast grating reflectors," *Opt. Express*, vol. 20, no. 18, pp. 20551–20557, 2012.

[145] Y. Wang, T. Wu, T. Tanae, H. Zhu, and K. Hane, "The resonant III-nitride grating reflector," *J. Micromech. Microeng.*, vol. 21, no. 10, p. 105025, 2011.

[146] Y. Wang, Z. Shi, X. Li, S. He, M. Zhang, and H. Zhu, "Surface-normal emission from subwavelength GaN membrane grating," *Opt. Express*, vol. 22, no. 1, pp. 667–672, 2014.

[147] J. Lee, S. Ahn, H. Chang, J. Kim, Y. Park, and H. Jeon, "Polarization-dependent GaN surface grating reflector for short wavelength applications," *Opt. express*, vol. 17, no. 25, pp. 22535–22542, 2009.

[148] T. T. Wu, S. H. Wu, T. C. Lu, and S. C. Wang, "GaN-based high contrast grating surface-emitting lasers," *Appl. Phys. Lett.*, vol. 102, no. 8, p. 081111, 2013.

[149] J. Laconte, D. Flandre, and J. P. Raskin, "Thin dielectric films stress extraction," *Micromachined Thin-Film Sensors for SOI-CMOS Co-Integration*, pp. 47–103, 2006.

[150] M. Rommel, B. Nilsson, P. Jedrasik, V. Bonanni, A. Dmitriev, and J. Weis, "Sub-10nm resolution after lift-off using HSQ/PMMA double layer resist," *Microelectron. Eng.*, vol. 110, pp. 123–125, 2013.

[151] S. Krishnamoorthy, D. N. Nath, F. Akyol, P. S. Park, M. Esposto, and S. Rajan, "Polarization-engineered GaN/InGaN/GaN tunnel diodes," *Appl. Phys. Lett.*, vol. 97, no. 20, p. 203502, 2010.

[152] S. Krishnamoorthy, F. Akyol, P. S. Park, and S. Rajan, "Low resistance GaN/InGaN/GaN tunnel junctions," *Appl. Phys. Lett.*, vol. 102, no. 11, p. 113503, 2013.

[153] D. Takasuka, Y. Akatsuka, M. Ino, N. Koide, T. Takeuchi, M. Iwaya, S. Kamiyama, and I. Akasaki, "GaInN-based tunnel junctions with graded layers," *Appl. Phys. Express*, vol. 9, no. 8, p. 081005, 2016.

[154] S. Krishnamoorthy, T. F. Kent, J. Yang, P. S. Park, R. C. Myers, and S. Rajan, "Gdn Nanoisland-Based GaN Tunnel Junctions," *Nano Lett.*, vol. 13, no. 6, pp. 2570–2575, 2013. PMID: 23662669.

[155] F. Akyol, S. Krishnamoorthy, and S. Rajan, "Tunneling-based carrier regeneration in cascaded GaN light emitting diodes to overcome efficiency droop," *Appl. Phys. Lett.*, vol. 103, no. 8, p. 081107, 2013.

[156] M. Malinverni, D. Martin, and N. Grandjean, "InGaN based micro light emitting diodes featuring a buried GaN tunnel junction," *Appl. Phys. Lett.*, vol. 107, no. 5, p. 051107, 2015.

[157] E. C. Young, B. P. Yonkee, F. Wu, S. H. Oh, S. P. DenBaars, S. Nakamura, and J. S. Speck, "Hybrid tunnel junction contacts to III-nitride light-emitting diodes," *Appl. Phys. Express*, vol. 9, no. 2, p. 022102, 2016.

[158] F. Akyol, S. Krishnamoorthy, Y. Zhang, J. Johnson, J. Hwang, and S. Rajan, "Low-resistance GaN tunnel homojunctions with 150 kA/cm^2 current and repeatable negative differential resistance," *Appl. Phys. Lett.*, vol. 108, no. 13, p. 131103, 2016.

[159] D. Adolph, R. R. Zamani, K. A. Dick, and T. Ive, "Hybrid ZnO/GaN distributed Bragg reflectors grown by plasma-assisted molecular beam epitaxy," *APL Mater.*, vol. 4, no. 8, 2016.

[160] D. Chen and J. Han, "High reflectance membrane-based distributed Bragg reflectors for GaN photonics," *Appl. Phys. Lett.*, vol. 101, no. 22, p. 221104, 2012.

[161] C. Zhang, S. H. Park, D. Chen, D. W. Lin, W. Xiong, H. C. Kuo, C. F. Lin, H. Cao, and J. Han, "Mesoporous GaN for Photonic Engineering? Highly Reflective GaN Mirrors as an Example," *ACS Photon.*, vol. 2, no. 7, pp. 980–986, 2015.

[162] Y. Zhang, S.-W. Ryu, C. Yerino, B. Leung, Q. Sun, Q. Song, H. Cao, and J. Han, "A conductivity-based selective etching for next generation GaN devices," *Phys. Stat. Sol. B*, vol. 247, no. 7, pp. 1713–1716, 2010.

[163] A. Altoukhov, J. Levrat, E. Feltin, J.-F. Carlin, A. Castiglia, R. Butté, and N. Grandjean, "High reflectivity airgap distributed bragg reflectors realized by wet etching of alinn sacrificial layers," *Appl. Phys. Lett.*, vol. 95, no. 19, p. 191102, 2009.

[164] S. Carlsson, "Towards high contrast gratings in the GaN/ZnO materials system," master's thesis, Chalmers University of Technology, Photonics Laboratory SE-41296 Gothenburg, 2013.

[165] Y. Zhang, B. Leung, and J. Han, "A liftoff process of GaN layers and devices through nanoporous transformation," *Appl. Phys. Lett.*, vol. 100, no. 18, p. 181908, 2012.

[166] D. Adolph and T. Ive, "Nucleation and epitaxial growth of ZnO on GaN (0001)," *Appl. Surf. Sci.*, vol. 307, pp. 438–443, 2014.

[167] M. Gębski, M. Dems, M. Wasiak, J. A. Lott, and T. Czyszanowski, "Monolithic subwavelength high-index-contrast grating VCSEL," *IEEE Photon. Technol. Lett.*, vol. 27, no. 18, pp. 1953–1956, 2015.

[168] Y. S. Liu, T. T. Kao, K. Mehta, S. C. Shen, P. D. Yoder, T. Detchprohm, R. D. Dupuis, H. Xie, and F. A. Ponce, "Development for ultraviolet vertical cavity surface emitting lasers," vol. 9748, pp. 974815–974815–7, 2016.

[169] J. T. Leonard, E. C. Young, B. P. Yonkee, D. A. Cohen, C. Shen, T. Margalith, T. K. Ng, S. P. DenBaars, B. S. Ooi, J. S. Speck, and S. Nakamura, "Comparison of nonpolar III-nitride vertical-cavity surface-emitting lasers with tunnel junction and ITO intracavity contacts," vol. 9748, pp. 97481B–97481B–13, 2016.

[170] M. Kneissl and J. Rass, eds., *III-Nitride Ultraviolet Emitters; Technology and Applications*, vol. 227. Springer International Publishing, 2016.

List of Acronyms

1D, 2D, 3D	one/two/three-dimensional
AFM	atomic force microscopy
BMP	beam propagation method
BOE	buffered oxide etch
CMP	chemical and mechanical polishing
CW	continuous-wave
DBR	distributed Bragg reflector
EBL	electron blocking layer
ECE	electrochemical etching
EEL	edge emitting laser
EIM	effective index method
ELO	epitaxial lateral overgrowth
FIB	focused ion beam
FS	free-standing
FWHM	full-width at half maximum
GMR	guided mode resonance
HAADF	high-angle annular dark-field
HCG	high contrast grating
hcp	hexagonal close-packed
ICP	inductively coupled plasma
LED	light emitting diode
LLO	laser lift-off
MBE	molecular beam epitaxy
MHCG	monolithic high contrast grating
NCTU	National Chiao Tung University
PEC	photoelectrochemical
PECVD	plasma-assisted chemical vapor deposition
PVD	physical vapor deposition
QCSE	quantum confined Stark effect
QW	quantum well
RCWA	rigorous coupled-wave analysis
RIE	reactive-ion etching
RT	room-temperature
SEM	scanning electron microscopy
SPSL	short-period superlattice
SSL	solid-state lighting
STEM	scanning transmission electron microscopy
TE	transverse-electric
TM	transverse-magnetic
TJ	tunnel junction
UCSB	University of California-Santa Barbara
UV	ultraviolet
VCSEL	vertical-cavity surface-emitting laser
VLC	visible light communication